MIKE 3 Wave Model FM

Hydrodynamic module

Validation Report

DHI A/S headquarters
Agern Allé 5
DK-2970 Hørsholm
Denmark

+45 4516 9200 Telephone
mike@dhigroup.com
www.mikepoweredbydhi.com

Company Registration No.: DK36466871

PLEASE NOTE

CONTENTS

MIKE 3 Wave Model FM
Hydrodynamic Module
Validation Report

1 Vision and scope

MIKE 3 Wave Model FM is a phase-resolving wave model based on the 3D Navier-Stokes equations and with the free surface described by a height function. The numerical techniques applied are based on an unstructured (flexible) mesh approach. A set of well-defined test cases for MIKE 3 Wave Model FM have been established. The test-suite is used for validation.

2 Methodology

2.1 Hardware

The validation tests have been performed using the following hardware platform:

Table 2.1 Hardware platform used for validation

	Computer	Processor	Memory	Operating system	GPUs
1	DELL Precision T7610 (workstation)	2 x Intel®Xeon® E5-2687W v2 (8 cores, 3.40 GHz)	32 GB	Windows 7 Professional SP1, 64-bit	2 x GeForce GTX Titan

2.2 Software

All validation tests have been performed using the Release 2019 version of the MIKE by DHI software.

3 Validation Test Cases

3.1 Standing Wave in a Deep Basin

3.1.1 Description

The standing wave test is a classic and good test for examining the numerical damping and long-term integration properties of the model. See Shi et al. (2012) and Lai et al. (2010)) for comparison.

Consider a small amplitude standing wave in a tank with flat bottom of length, L. and depth, d. We assume no variations in the y-direction and linear, irrotational and inviscid conditions under which the governing equations reduce to:

$$\frac{\partial u}{\partial t} = -\frac{1}{\rho_0}\frac{\partial p}{\partial x}, \qquad \frac{\partial w}{\partial t} = -\frac{1}{\rho_0}\frac{\partial p}{\partial z}, \qquad \frac{\partial u}{\partial x} + \frac{\partial w}{\partial z} = 0,$$

Where the total pressure $p = \rho_0 g\eta + q$ is the sum of the hydrostatic pressure and the non-hydrostatic pressure, q. The boundary conditions for the non-hydrostatic pressure are $q = 0$ at the surface and $\partial q/\partial n = 0$ on walls and bottom where n is the normal vector. Free-slip conditions are assumed for the velocity field.

Let the initial surface elevation at time $t = 0$ be:

$$\eta_0 = A_0 \cos(kx)$$

where $k = 2\pi/\lambda$ is the wave number, λ is the wave length and A_0 is the amplitude.

The analytic solution to the problem is then:

$$\eta(x,t) = A_0 \cos(kx)\cos(\omega t)$$

$$q(x,z,t) = \rho_0 g A_0 (\varphi(z) - 1)\cos(kx)\cos(\omega t)$$

$$u(x,z,t) = g A_0 \frac{k}{\omega}\varphi(z)\sin(kx)\sin(\omega t)$$

$$w(x,z,t) = -g A_0 \frac{1}{\omega}\frac{\partial \varphi(z)}{\partial z}\cos(kx)\sin(\omega t)$$

where the angular frequency is $\omega^2 = gk\tanh(kd)$ by the linear dispersion relation and the vertical distribution used above is:

$$\varphi(z) = \tanh(kd)\sinh(kz) + \cosh(kz)$$

The phase speed and period of the wave are:

$$c = \sqrt{(g/k)\tanh(kd)}, \qquad T = \frac{\lambda}{c}$$

3.1.2 Set-up

We consider a test with a uni-modal standing wave, meaning $\lambda = 2L$, in a $L = 10$m long basin with depth $d = 10$m, 20m and 40m and a width of 1m. The amplitude of the standing wave is $A_0 = 0.001$m to ensure linear conditions. The theoretical phase speed and period are shown in Table 3.1.

Table 3.1 The theoretical phase speed and period

d (m)	kh (m)	Theoretical		Hydrostatic assumptions	
		c (m/s)	T (s)	c (m/s)	T (s)
5	1.5708	5.351560	3.737228	7.003570	2.85568
10	3.1416	5.577616	3.585761	9.904544	2.01927
20	6.2832	5.588021	3.579084	14.007141	1.42784
40	12.5664	5.588040	3.579071	19.809088	1.00963

To verify the convergence of the model a number of different set-ups are tested. The horizontal mesh consists of uniform quadrilateral elements with an edge length of 0.25m resulting in 160 elements. Simulations have also been performed using unstructured triangular meshes, which consist of 163 and 623 elements. The mesh with 623 elements is shown in Figure 3.1. The numbers of sigma layers are 3, 5, 10, 20 and 40. Both equidistant and non-equidistant (sigma_c=0.1, b=0 and theta=2) vertical discretization are applied. The non-equidistant vertical discretization is illustrated in Figure 3.2. The simulation period is 600s.

The simulations are performed without Riemann solver. No horizontal or vertical eddy viscosity or bed resistance have been applied.

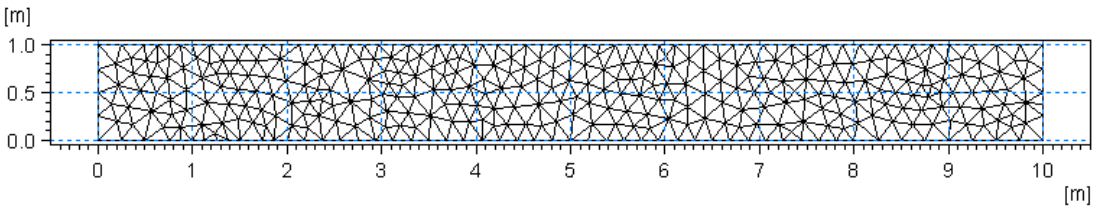

Figure 3.1 Unstructured triangular mesh with 623 elements.

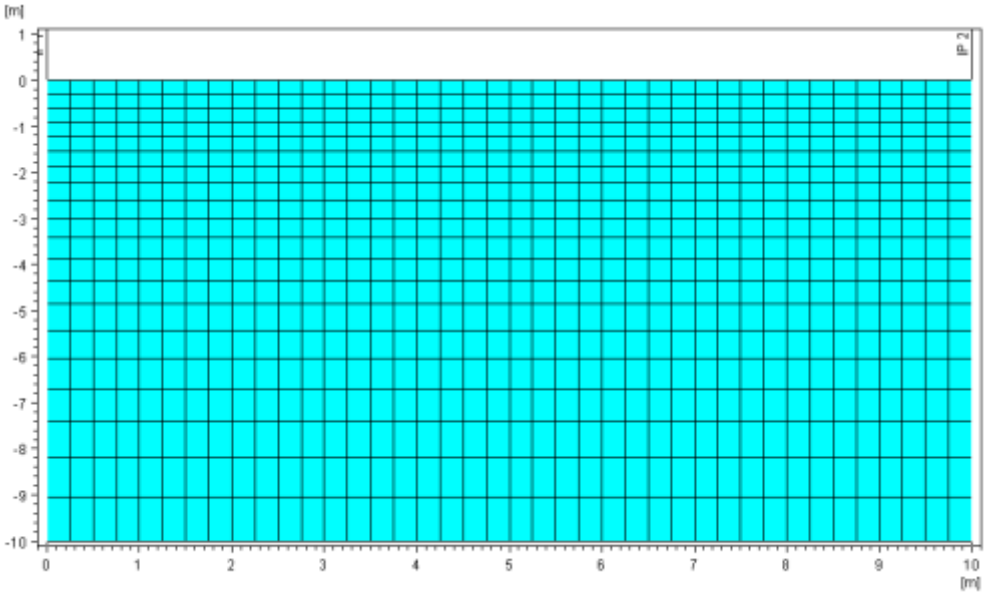

Figure 3.2 Cross section for the structured mesh with 20 non-equidistant vertical layers.

3.1.3 Results

A snapshot of the non-hydrostatic pressure after 12.5s can be seen in Figure 3.3.

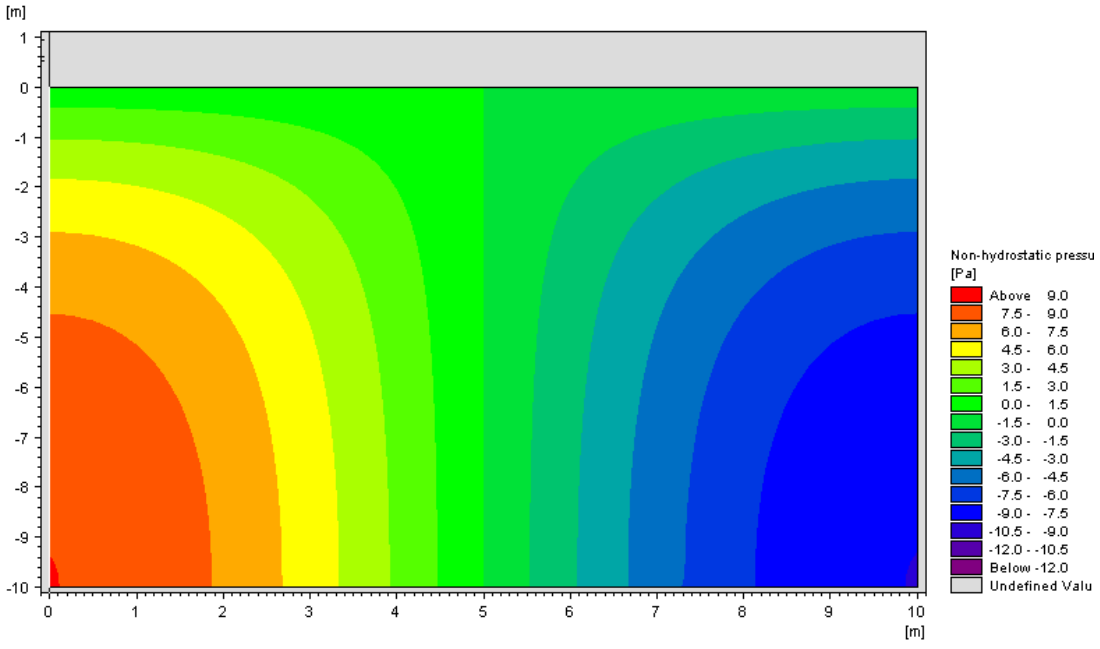

Figure 3.3 A snapshot of the non-hydrostatic pressure in the standing wave test after 12.5s.

Figure 3.4 and Figure 3.5 show plots of the wave period error as function of the number of vertical layers. In Figure 3.4 the equidistant vertical discretization and the structured mesh is used, and in Figure 3.5 the non-equidistant vertical discretization and the structured mesh is used.

It is seen that the error decreases fast with an increased number of layers and that non-equidistant discretization significantly improves the accuracy. In Figure 3.6 time series of the surface elevation in the right end of the tank is plotted against the analytic solution. It is seen that the amplitude error is very small. Figure 3.7 shows a plot of the wave period error as function of the number of vertical layers for the case with water depth 10m and unstructured mesh.

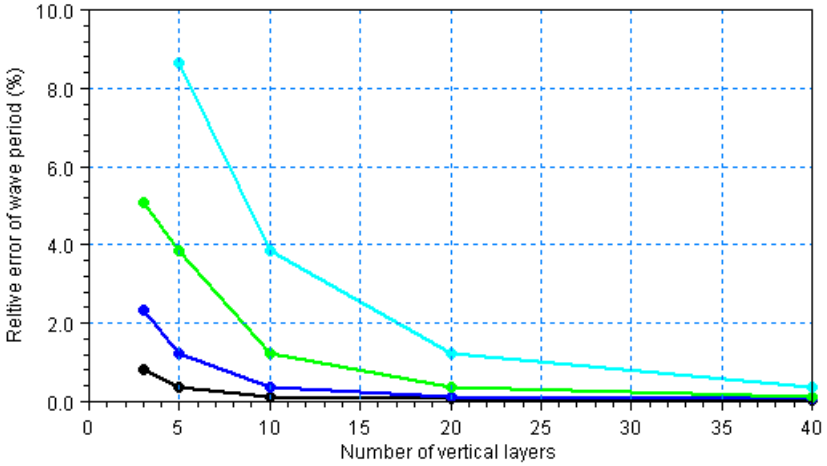

Figure 3.4 Wave period errors (%) for the standing wave test with quadrilateral elements and equidistant vertical discretization. Black curve: d=5m; blue curve: d=10m; green curve: d=20m; light blue: d=40m.

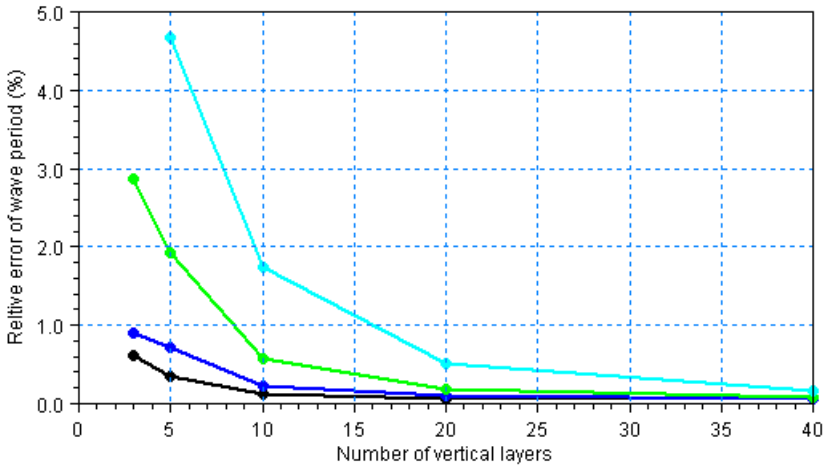

Figure 3.5 Wave period errors (%) for the standing wave test with quadrilateral elements and non-equidistant vertical discretization. Black curve: d=5m; blue curve: d=10m; green curve: d=20m; light blue: d=40m.

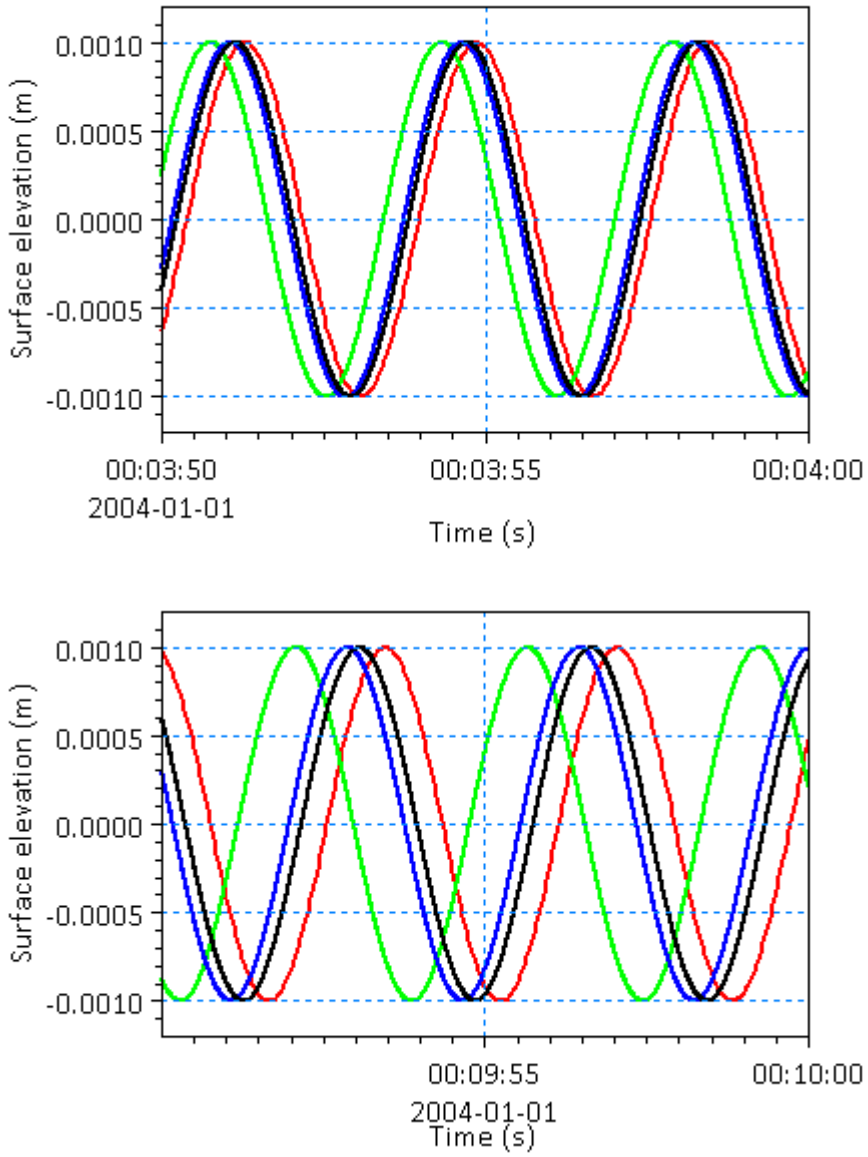

Figure 3.6 Surface elevation at the right end of the tank for the standing wave test case with water depth 10m, structured mesh and various numbers of non-equidistant vertical layers. Green curve: 10 layers; Blue line: 20 layers; Black line: 40 layers; Red line: Analytical solution.

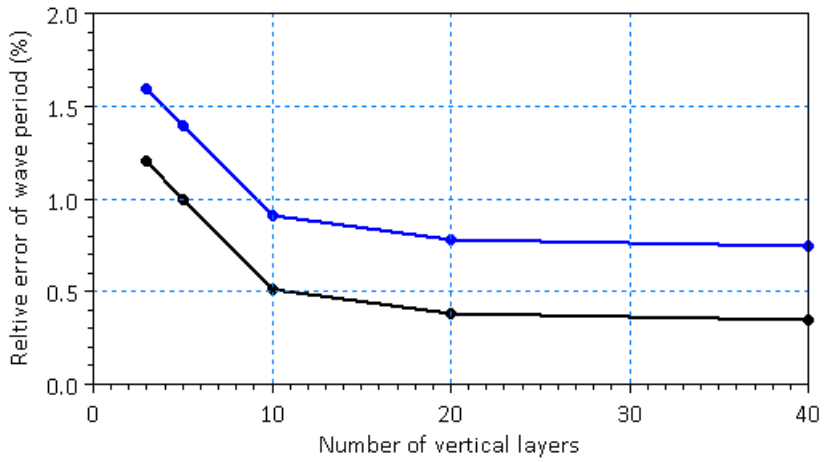

Figure 3.7 Wave period errors (%) for the standing wave test with water depth 10m, triangular elements and non-equidistant vertical discretization. .Blue curve: coarse mesh (163 elements); black curve: fine mesh (623 elements).

3.2 Propagation of Regular waves over a Submerged Bar

3.2.1 Description

Wave transformation over a submerged bar is a very demanding test case for most wave models as it involves non-linear shoaling and growth of bound harmonics on the uphill slope and subsequent release of higher harmonics on the downhill slope. After the bar, these harmonics will propagate as free waves. Luth et al. (1994) performed a series of accurate flume experiments for wave transformation over a trapezoidal bar with an upward slope of 1/20, a downward slope of 1/40, a constant depth of 0.4m before and after the bar and a depth of 0.1m on top of the bar (see Figure 3.8). As an example from the test series is selected the case for regular nonbreaking waves with wave period 2.02s and wave height 0.02m.

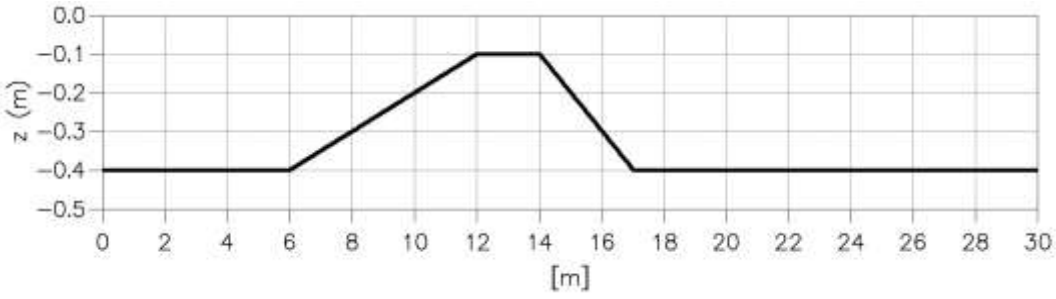

Figure 3.8 Bed profile.

3.2.2 Setup

This test case is a one-dimensional flow problem. Hence, a one-element wide channel is used in the simulation. The horizontal mesh consists of quadrilateral elements with an edge length of 0.02m. In the vertical 3, 5, and 10 non-equidistant (sigma_c=0.0, b=0 and theta=2.7) sigma layers are used. A simulation is also performed with 3 equidistant sigma layers. The incoming waves are specified using a relaxation zone: Line from (x,y)=(2.0m,

0.05m) to (x,y)=(2.0m, 0.0) and the width of the ramp-up zone is 1.8m. The waves are generated using Stokes 5th order wave theory. The outgoing waves at the downstream boundary are absorbed using a 4m wide sponge layer.
Simulations have been performed without the Riemann solver. No horizontal or vertical eddy viscosity has been applied.

3.2.3 Results

In Figure 3.9-Figure 3.12 the measured time series of surface elevations at x=13.5m, x=17.3m, x=19.0m and x=21.0m is compared to the numerical results using MIKE 3 Wave Model FM with 10 non-equidistant sigma layers. MIKE 3 Wave model FM is seen to provide highly accurate results. In Figure 3.13 the measured surface elevation at x=21.0m is compared to the numerical results using MIKE 3 Wave Model FM with 3, 5, and 10 non-equidistant sigma layers, respectively. Figure 3.14 shows the amplitude for the measured and the computed higher harmonics along the channel.

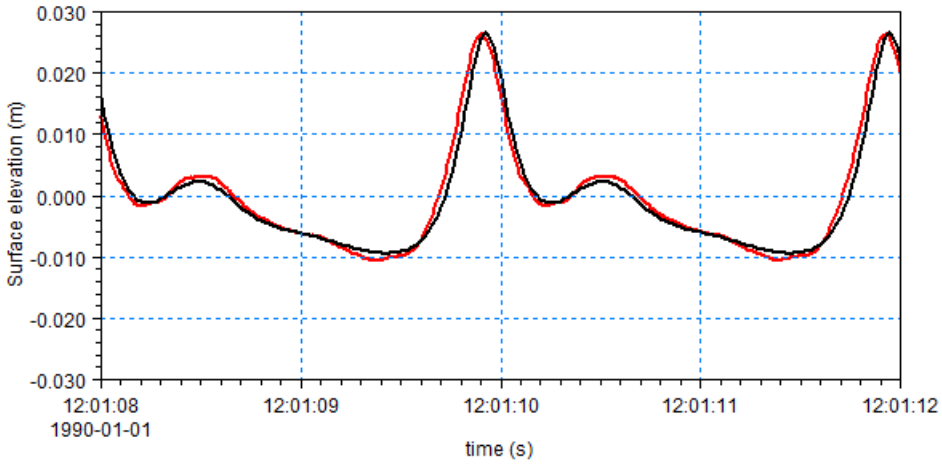

Figure 3.9 Computed and measured surface elevation at x=13.5m. Black line: MIKE 3 Wave Model FM with 10 non-equidistant sigma layers; Red line: Experimental data.

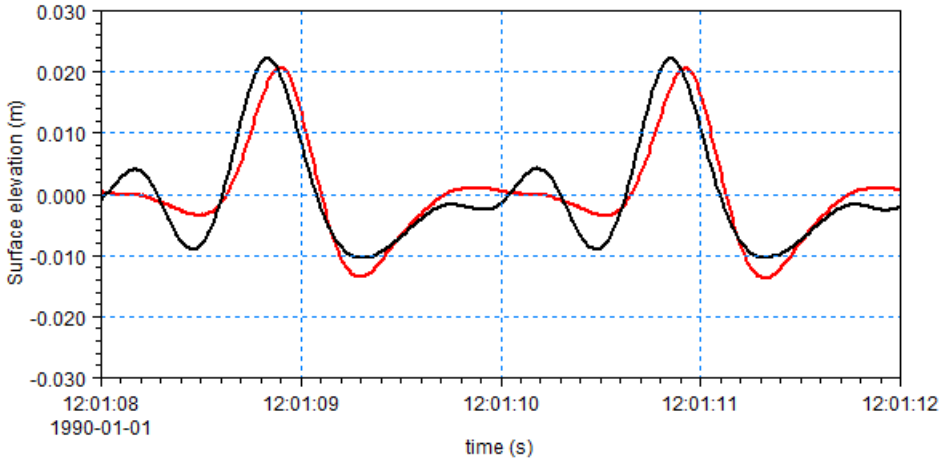

Figure 3.10 Computed and measured surface elevation at x=17.3m. Black line: MIKE 3 Wave Model FM with 10 non-equidistant sigma layers; Red line: Experimental data.

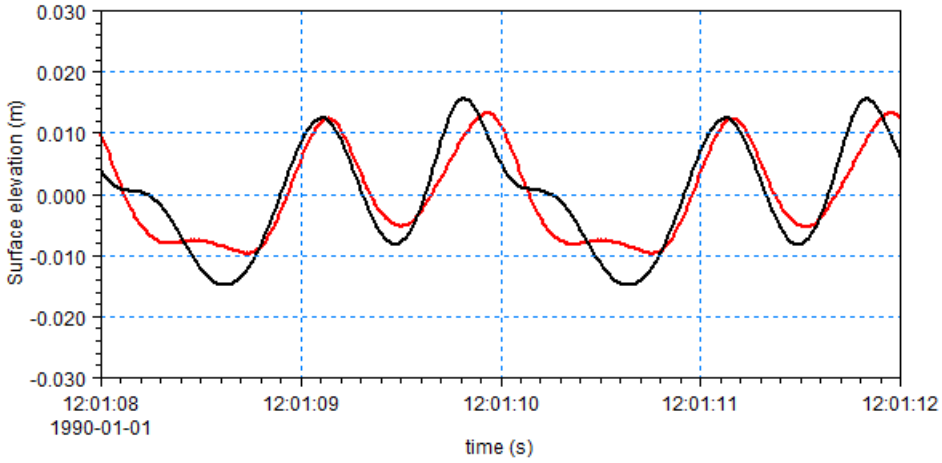

Figure 3.11 Computed and measured surface elevation at x=19.0m. Black line: MIKE 3 Wave Model FM with 10 non-equidistant sigma layers; Red line: Experimental data.

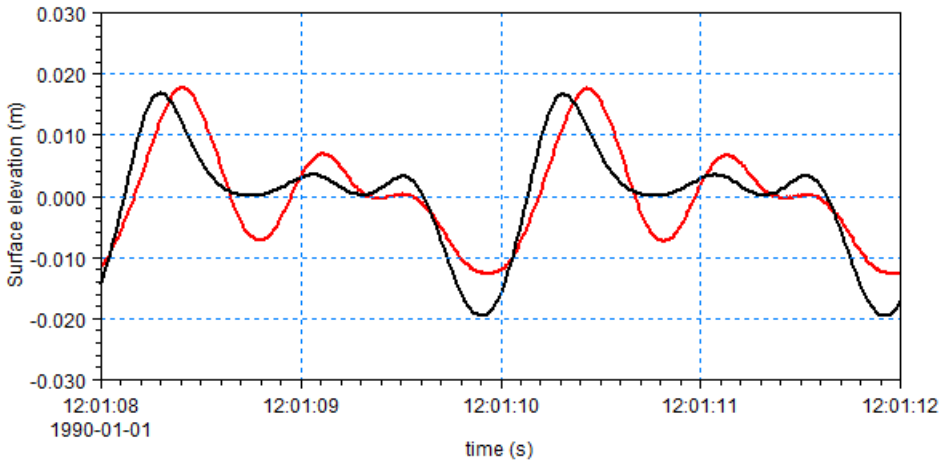

Figure 3.12 Computed and measured surface elevation at x=21.0m. Black line: MIKE 3 Wave Model FM with 10 non-equidistant sigma layers; Red line: Experimental data.

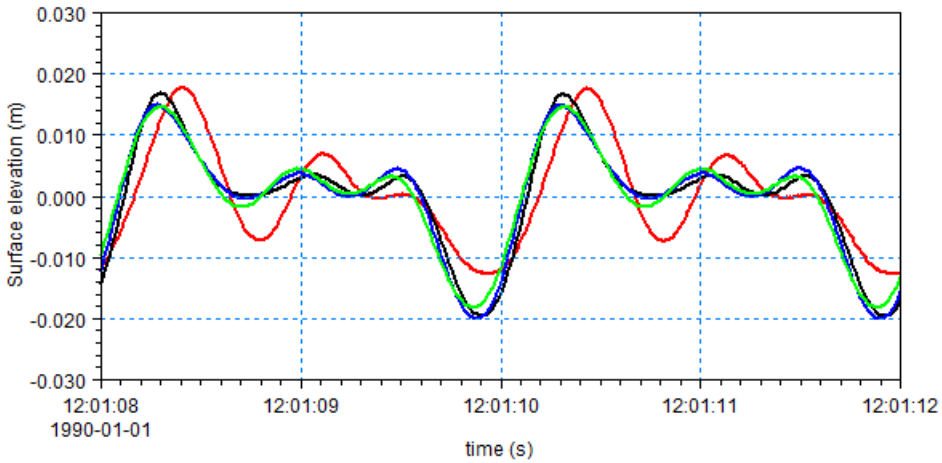

Figure 3.13 Computed and measured surface elevation at x=21.0m. Green line: MIKE 3 Wave Model FM with 3 non-equidistant sigma layers; Blue line: MIKE 3 Wave Model FM with 5 non-equidistant sigma layers; Black line: MIKE 3 Wave Model FM with 10 non-equidistant sigma layers; Red line: Experimental data.

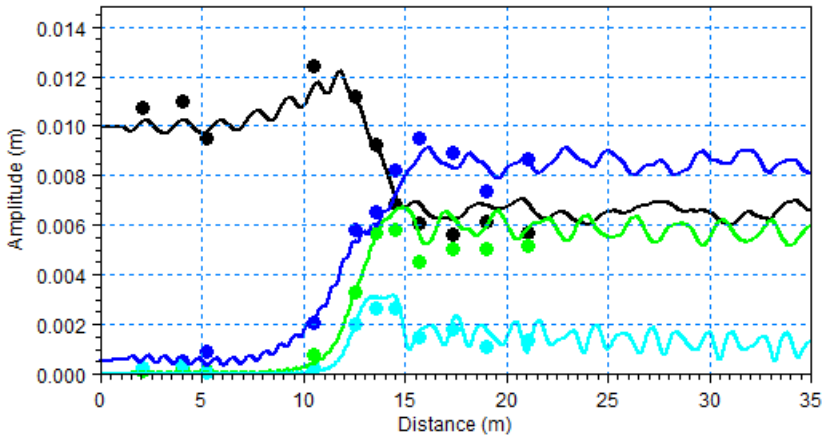

Figure 3.14 Wave amplitude for the higher harmonic along the channel. Black: First harmonic; Blue: Second harmonic.; Green: Third harmonic; Light blue: Forth harmonic; Solid line: Numerical calculations. Circles: Experimental data.

3.3 Non-linear Refraction-Diffraction of Regular Waves over a Semicircular Shoal

3.3.1 Description

This test case is the non-linear refraction-diffraction of regular waves over a semicircular shoal. The problem was studied experimentally by Whalin (1971). For a presentation of numerical results, see e.g. Madsen and Sørensen (1992) and the references herein. The model area covers 6.096m x 36.576m with a depth variation given by

$$h(x,y)=\begin{cases}0.4572 & 0\le x\le 10.67-G\\ 0.4572+\dfrac{1}{25}(10.67-G-x) & 10.67-G\le x\le 18.29-G\\ 0.1524 & 18.29-G\le x\le 36.576\end{cases}$$

where

$$G(y)=\left[y(6.096-y)\right]^{1/2} \qquad 0\le y\le 6.096)$$

Whalin performed a series of experiments with different wave conditions. Here, calculations are performed for the case with a wave period of 2s and a wave amplitude of 0.0075m.

3.3.2 Setup

Both a structured and an unstructured mesh are used. The length of the domain is extended with 1.524m to account for the relaxation zone. The horizontal structured mesh consists of uniform quadrilateral elements with an edge length of 0.0508m, resulting in 90120 elements. The horizontal unstructured mesh consists of 89953 triangular elements. A non-equidistant (sigma_c=0.1, b=0 and theta=2) vertical discretization with 5 layers is applied. The incoming waves are specified using a relaxation zone: Line from (x,y)=(0.0m,

6.1m) to (x,y)=(0.0m, 0.0) and the width of the ramp-up zone is 1m. The waves are generated using stream function wave theory. The outgoing waves at the downstream boundary are absorbed using a 6m wide sponge layer. No horizontal or vertical eddy viscosity has been applied.

The simulations using structured mesh are performed without Riemann solver. For the simulations with unstructured mesh the HLLC solver is used with a Riemann factor of 0.05.

3.3.3 Results

The incoming waves are linear, but after the focusing on the shoal, higher harmonics become significant due to non-linear effects. The focusing of the waves can be seen in Figure 3.15 showing an instantaneous surface elevation field calculated using the structured mesh. In Figure 3.16 the surface elevation along the centreline is shown using the two meshes. The energy transfer to higher harmonics is illustrated in Figure 3.17. Based on a Fourier analysis of the time series of the surface elevation at each grid point along the centreline, the spatial evolution of the first, second and third harmonics from the numerical simulations is compared with the experimental data. The results using the structured and the unstructured mesh are almost identical and the agreement with the measurements is quite good.

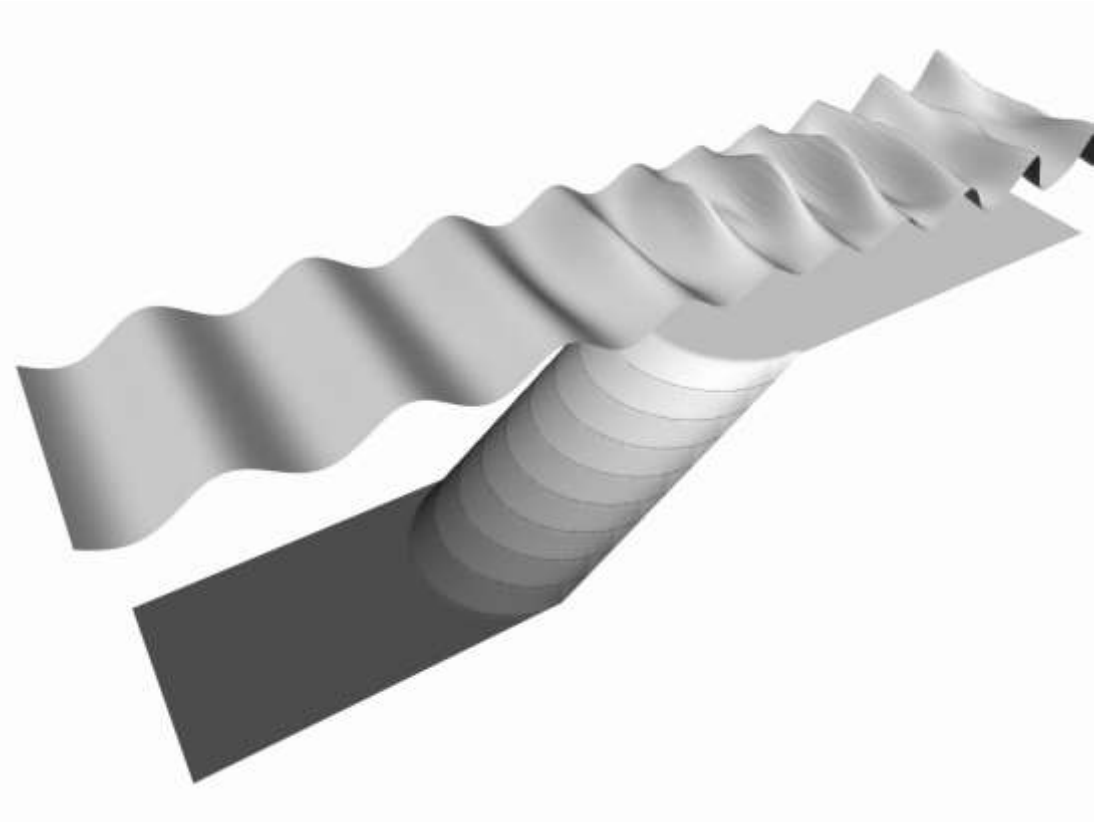

Figure 3.15 Instantaneous surface elevation calculated using structured mesh shown over the bathymetry.

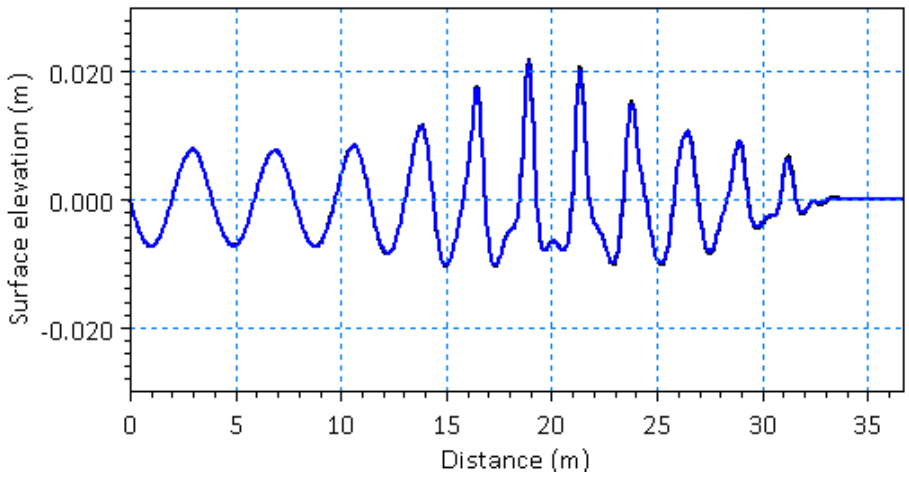

Figure 3.16 Surface elevation along the centreline (T = 2s and H = 0.015m). Black line: structured mesh; Blue line: Unstructured mesh.

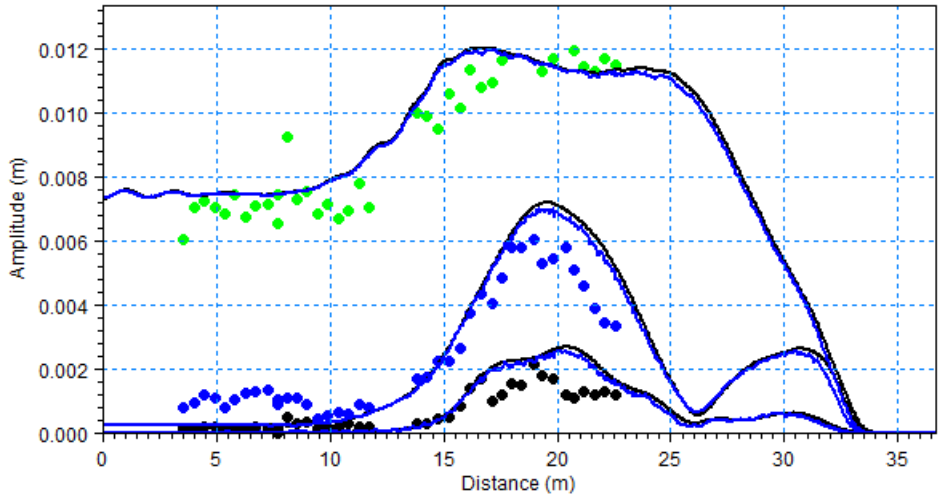

Figure 3.17 Wave amplitude for the first, second and third harmonic along the centreline. (T = 2s and H = 0.015m). Black line: Structured mesh; Blue line: unstructured mesh.; Green, blue and black circles: Experimental data by Whalin (1971) for first, second and third harmonics.

3.4 Wave Runup on a Gently Sloping Beach

3.4.1 Description

The test case is widely used in connection with calculation of short waves using higher order models, such as Boussinesq models. See e.g. Madsen et al. (1997). The case shows the ability of the MIKE Wave Model FM series to handle flooding and drying on a sloping bottom.

The computational domain is 15m long with a constant slope of 1:25. The west (deepest end) boundary has the depth of 0.5m at mean water level. A wave with amplitude of 0.003m and a period of 10s is applied to the west boundary.

An analytical solution exists for the case. See e.g. Carrier and Greenspan (1958).

3.4.2 Setup

Both a structured and an unstructured mesh are used. The horizontal meshes cover a domain of 5m by 15m. The structured mesh consists of 7500 uniform quadrilateral elements with an edge length of 0.1m. The unstructured mesh consists of 10405 triangular elements. The elements vary in size, the largest being approximately 0.04m2 in the deepest end and the smallest being approximately 0.003m2 in the shallow end. The grid is seen in Figure 3.18. For the vertical discretization 5 equidistant sigma layers are used. The incoming waves are specified using a relaxation zone: Line from (x,y)=(0.5m, 5.0m) to (x,y)=(0.5m, 0.0) and the width of the ramp-up zone is 0.4m. The waves are generated using 1st order Stokes theory.

Simulations have been performed using the HLLC solver. No horizontal or vertical eddy viscosity has been applied.

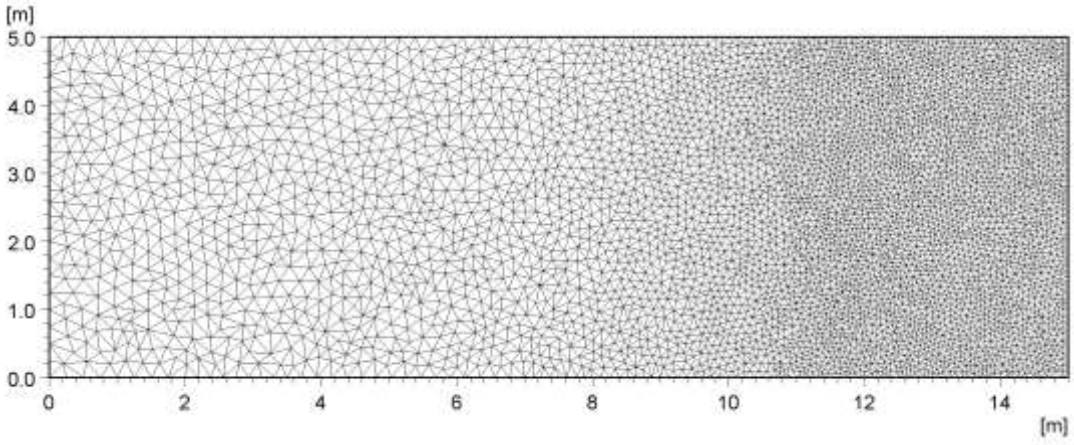

Figure 3.18 Computational mesh used in the wave on a sloping beach case.

3.4.3 Results

The results are shown in Figure 3.19 and
Figure 3.20. As seen, the results using both the structured and the unstructured mesh are in very good agreement with the analytical solution.

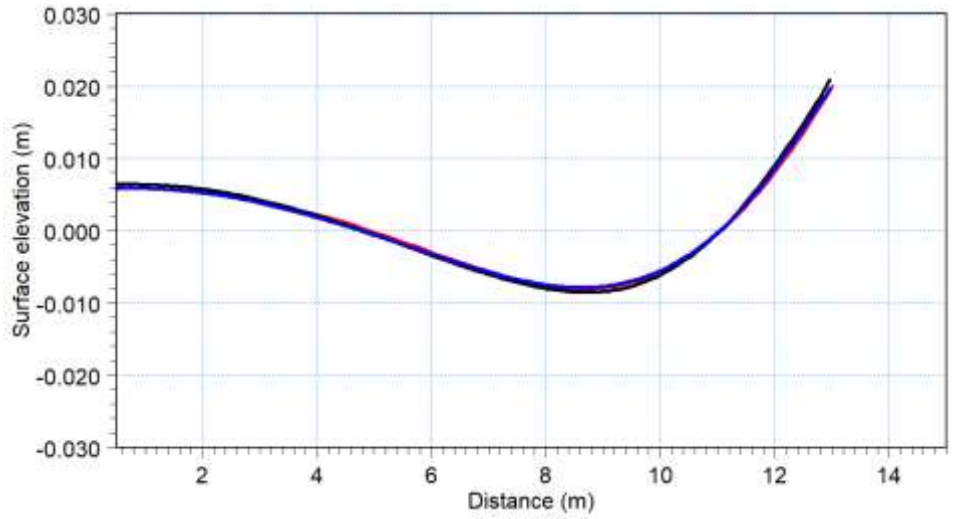

Figure 3.19 Cross-shore variation of surface elevation at the maximum elevation on the boundary. Black line: MIKE 3 Wave Model FM (structured mesh); Blue line: MIKE 3 Wave Model FM (unstructured mesh); Red line: Analytical solution.

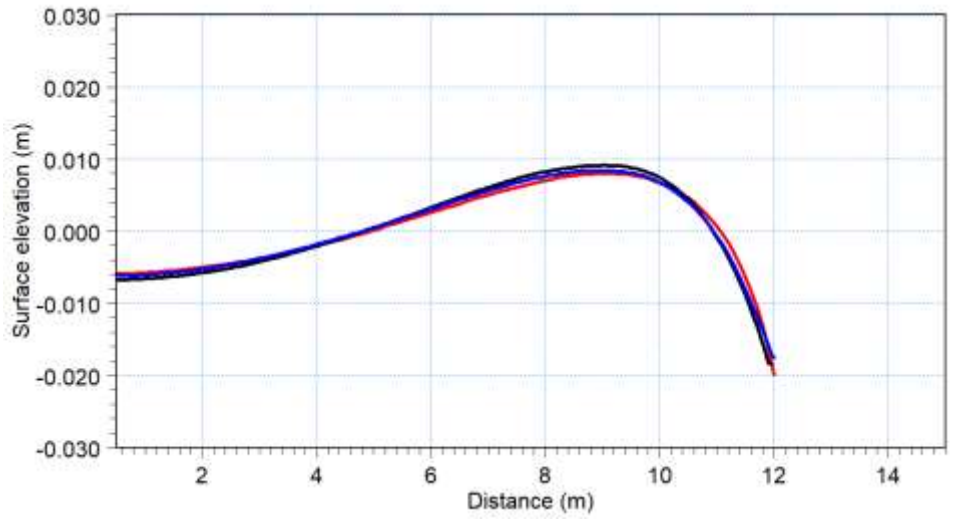

Figure 3.20 Cross-shore variation of surface elevation at the minimum elevation on the boundary. Black line: MIKE 3 Wave Model FM (structured mesh); Blue line: MIKE 3 Wave Model FM (unstructured mesh); Red line: Analytical solution.

3.5 Shoaling and Breaking of Regular Waves on a Gently Sloping Beach

3.5.1 Description

Ting and Kirby (1994) presented measurements for both spilling breakers and plunging breakers on a plane sloping beach with a slope of 1/35 starting at a depth of 0.40m. The numerical setup is shown in Figure 3.21. As input, they generated for the spilling breakers case regular waves with a period of 2.0s and a wave height of 0.125m and for the plunging breaker case regular waves with a period of 5.0s and a wave height of 0.128m.

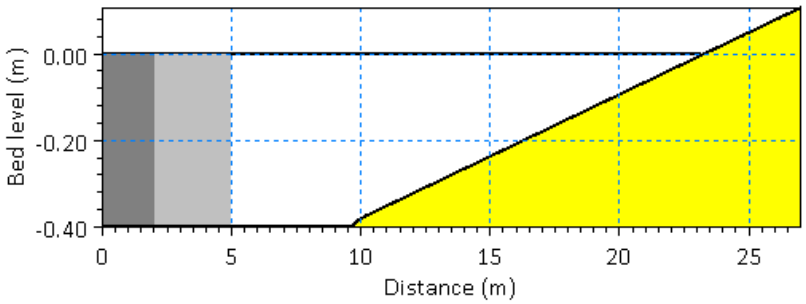

Figure 3.21 Sketch illustrating numerical setup.

3.5.2 Setup

This test case is a one-dimensional flow problem. Hence, a one-element wide channel is used in the simulation. The horizontal mesh consists of quadrilateral elements with an edge length of 0.02m are. An equidistant vertical discretization with 12 layers is applied. The incoming waves are specified using a relaxation zone: Line from (x,y)=(5.0m, 0.02m) to (x,y)=(5.0m, 0.0) and the width of the ramp-up zone is 3.0m. The waves are generated using the stream function wave theory.

Simulations have been performed using the HLLC solver. Both horizontal and vertical eddy viscosity have been applied using the k-epsilon formulation. Bed friction is applied with a roughness height of 0.0005.

3.5.3 Results

The cross-shore variation of the wave crest elevation, wave trough elevation and mean water level are shown in Figure 3.22 and Figure 3.23.

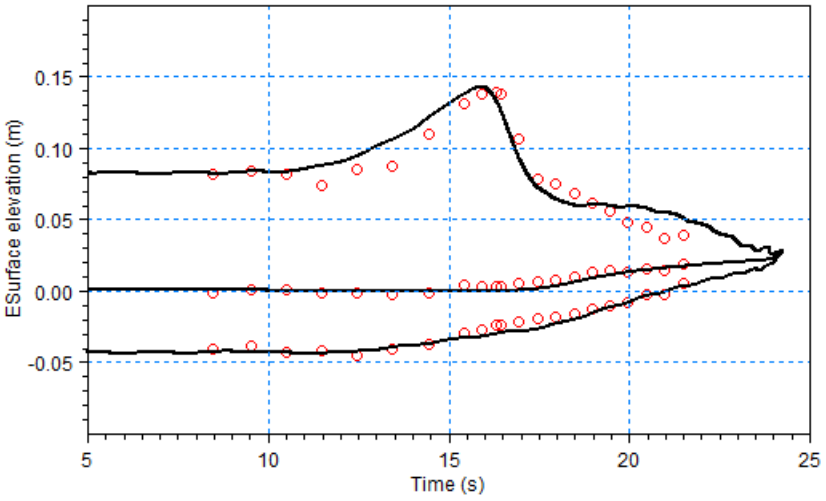

Figure 3.22 The cross-shore variation of the wave crest elevation, wave trough elevation and mean water level for the test of Ting and Kirby (1994) with spilling breakers (T=2s). Black line: MIKE 3 Wave Model FM; Red circles; experimental data.

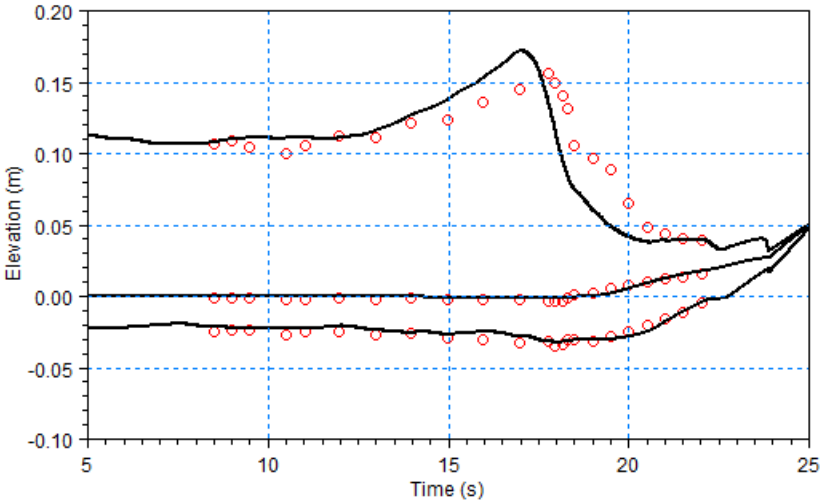

Figure 3.23 The cross-shore variation of the wave crest elevation, wave trough elevation and mean water level for the test of Ting and Kirby (1994) with plunging breakers (T=5s). Black line: MIKE 3 Wave Model FM; Red circles; experimental data.

The modelled and measured undertow is compared in Figure 3.24. The locations of the measurements at position A–H are at x = [8.735m, 15.945m, 16.665m, 17.275m, 17.885m, 18.495m, 19.110m, 19.725m]. The last six locations are within the surf zone. It is seen that MIKE 3 Wave Model FM does a fair job predicting the undertow at A, F, G and H. At locations B, C, D and E the model over-predicts the undertow velocities in the lower part of the water. This is likely related to the wave being too large before breaking and breaking slightly further off-shore in MIKE 3 Wave Model FM compared to the measurements. The vertical discretization is also too coarse to resolve the vertical variation in the flow.

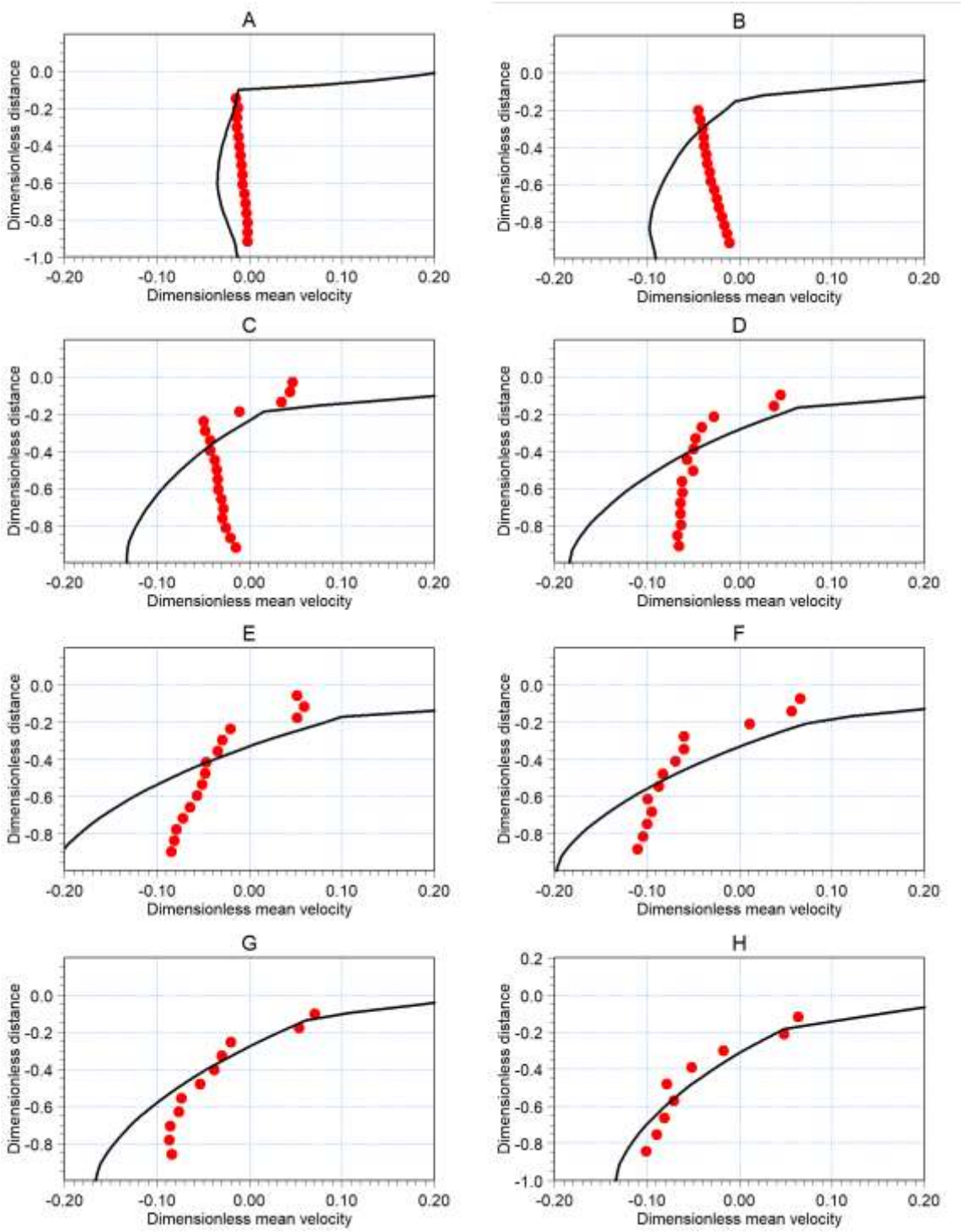

Figure 3.24 Comparison between measured and modelled undertow at the 8 locations. Black line: MIKE 3 Wave Model FM; Red circles; experimental data. The dimensionless mean velocity is defined by u_mean/√(gh_mean) and the dimensionless distance is defined by (z-s_(mean))/h_mean.The mean water depth, hmean is determined as the still water depth plus the calculated mean surface elevation, smean, and umean is the calculated mean velocity.

3.6 Rip Channel

3.6.1 Description

Laboratory experiments for a case with waves propagation on a plane beach with a rip channel have been reported by Hamm (1992a,b). The wave basin is 30m x 30m and the bathymetry is a plane sloping beach of 1:30 with a rip channel excavated along the centreline. The depth variation is given by

$$h(x,y)=\begin{cases}0.5 & x\le 7\\ -0.1+\dfrac{25-x}{30}\left[1+3\exp\left(-\dfrac{25-x}{3}\right)\cos^{10}\left(\dfrac{\pi(15-y)}{30}\right)\right] & 7<x<25\\ -0.1+\dfrac{25-x}{30} & x\le 25\end{cases}$$

Hamm considered a number of different incident wave conditions. Here the case with unidirectional, regular, incident waves with a period of 1.25s and a wave height of 0.07m is considered.

3.6.2 Setup

Only half of the physical wave tank is covered in the computations, and reflective boundary conditions are applied at the line of symmetry. Simulations are performed using both a structured mesh with 80000 elements and an unstructured mesh also with 80000 elements. The incoming waves are specified using a relaxation zone: Line from (x,y)=(2.0m, 15.0m) to (x,y)=(2.0m, 0.0) and the width of the ramp-up zone is 1.0m. The waves are generated using stream function wave theory. The simulation period is 300s corresponding to 240 wave periods.

Simulations are performed using the HLLC solver with a Riemann factor of 0.25. For the horizontal eddy the Smagorinsky formulation is used with a Smagorinsky factor of 0.28 and for the vertical eddy the k-epsilon formulation is used. Bed friction is applied with a roughness height of 0.005m.

3.6.3 Results

Due to the difference in the wave set-up along the rip channel, and at the plane beach away from the rip channel there is an alongshore gradient in the mean water surface elevation. This gradient will force a current towards the centreline. The flow from both sides will join to form a rip current and two symmetrical circulation cells will be created. A steady-state current field will be reached when the forcing due to the gradient in the mean surface elevation is balanced out by the bed friction.

Figure 3.25 shows the cross-shore variation of the wave height at some distance from the rip channel where the beach is a plane slope. A plot along the excavated beach at the centreline is shown in Figure 3.26. The measurements of Hamm are included and the agreement is quite good. A vector plot of the time-averaged velocity field is shown in Figure 3.27 and Figure 3.28 for the mesh with quadrilateral elements and triangular

elements. A subdomain is shown in order to focus on the circulation cell. The velocity is computed as the time-average of the depth-average velocity. The velocity vectors are shown in a structured grid. A pronounced rip current is seen along the centreline of the bathymetry, i.e. at the top of the figure. A formation of small eddies along the plane beach can also be identified. However, more detailed data are needed to show if similar eddies are actually present in the physical experiment. The cross-shore variation of the velocity along the centreline is shown in Figure 3.29. The maximum current speed is 0.14m/s for the simulation using quadrilateral elements and 0.15m/s for the simulation using triangular elements. In Figure 3.30 is show the calculated mean u-velocity I a vertical plane along the centreline.

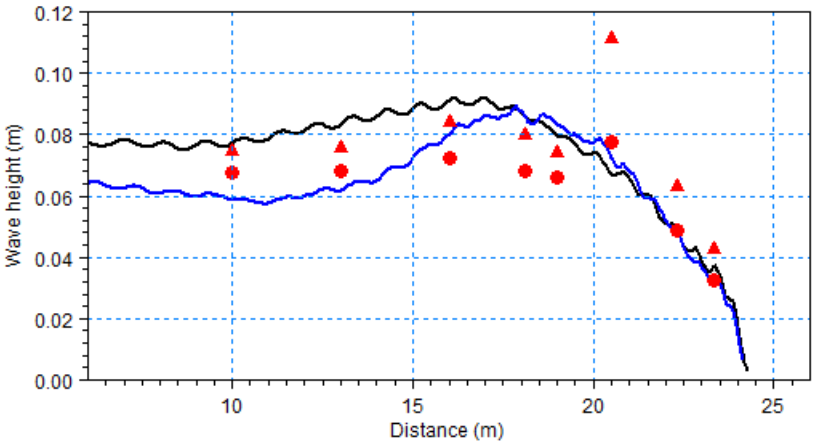

Figure 3.25 Comparison between the computed and measured cross-shore variation of the wave height. Black line: MIKE 3 Wave Model FM (structured mesh); Blue line: MIKE 3 Wave Model FM (unstructured mesh). ▲ Experimental data by Hamm (1992b) - Significant wave height, $H_{1/3}$: ● Experimental data by Hamm (1992b) - Variance-based wave height $H_\sigma/\sqrt{2}$.

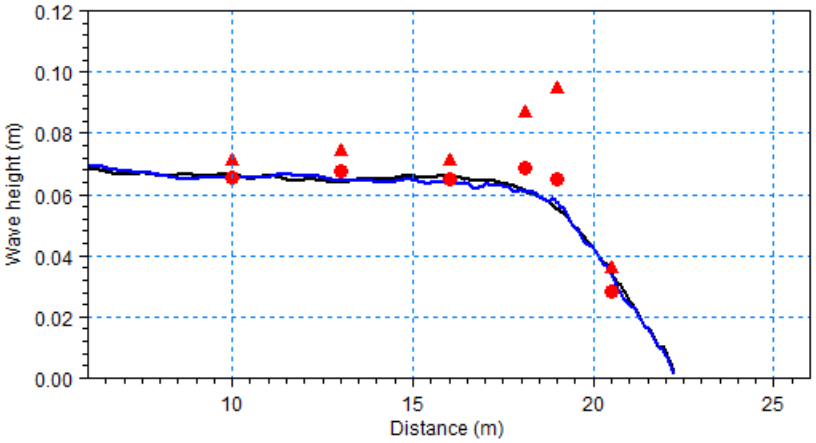

Figure 3.26 Comparison between the computed and measured cross-shore variation of the wave height. Black line: MIKE 3 Wave Model FM (structured mesh); Blue line: MIKE 3 Wave Model FM (unstructured mesh). ▲ Experimental data by Hamm (1992b) - Significant wave height, $H_{1/3}$; ● Experimental data by Hamm (1992b) - Variance-based wave height $H_\sigma/\sqrt{2}$.

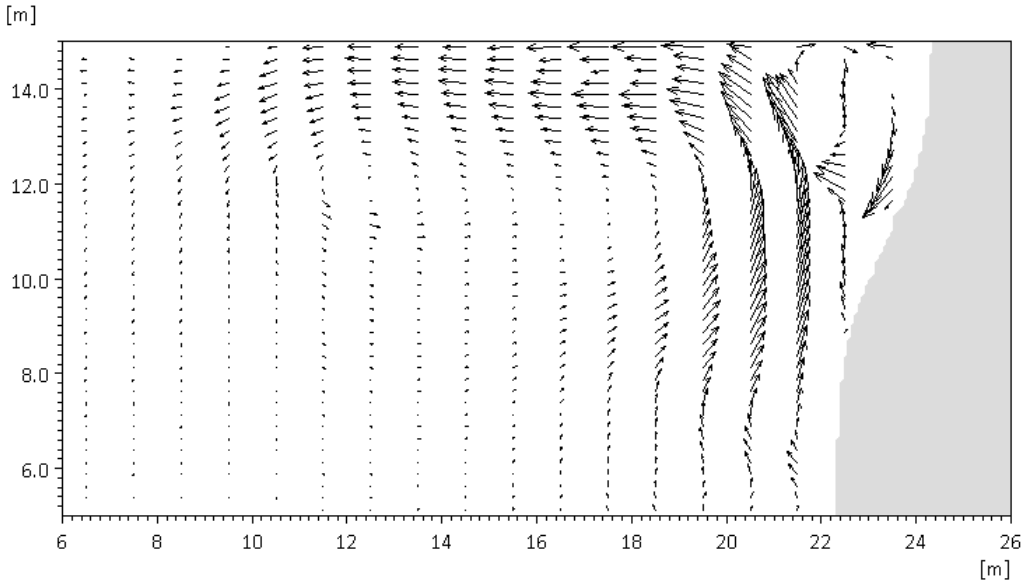

Figure 3.27 Depth-averaged velocity focusing on the circulation cell. Mesh with quadrilateral elements.

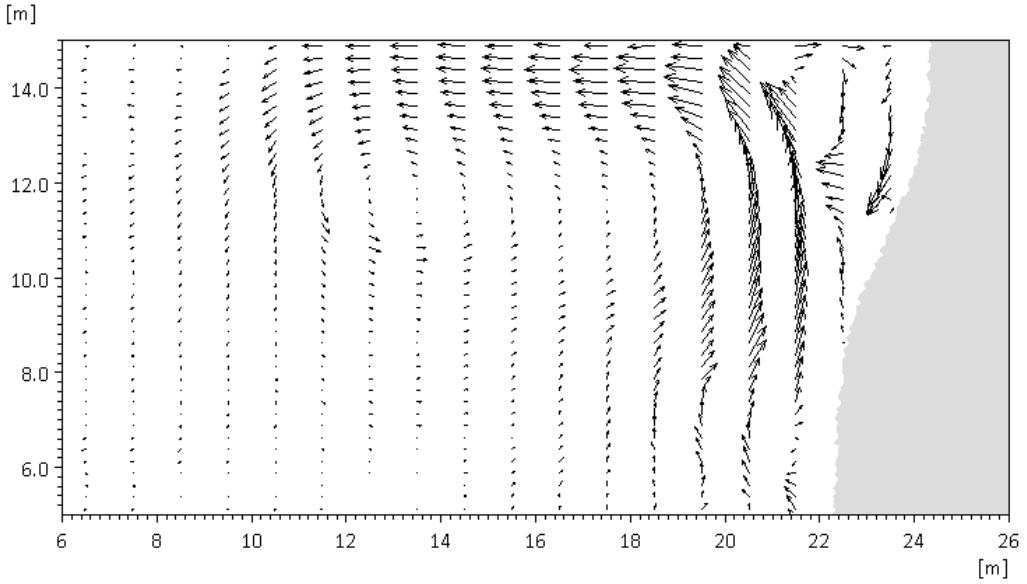

Figure 3.28 Depth-averaged velocity focusing on the circulation cell. Mesh with triangular elements.

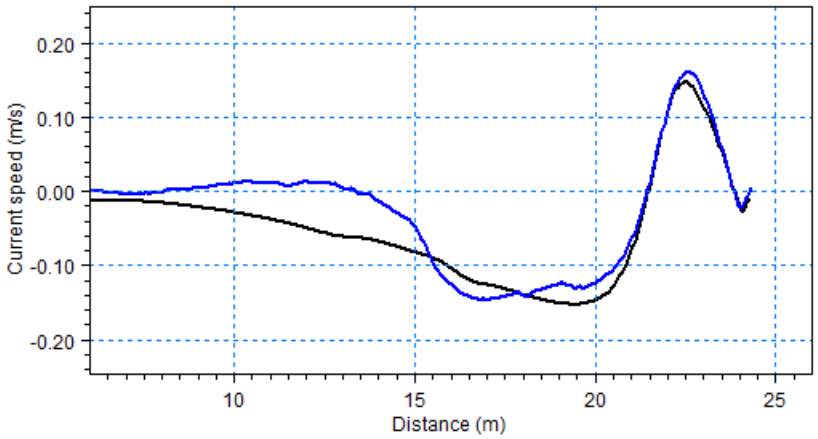

Figure 3.29 Rip current along the centreline. Black line: MIKE 3 Wave Model FM (structured mesh); Blue line: MIKE 3 Wave Model FM (unstructured mesh).

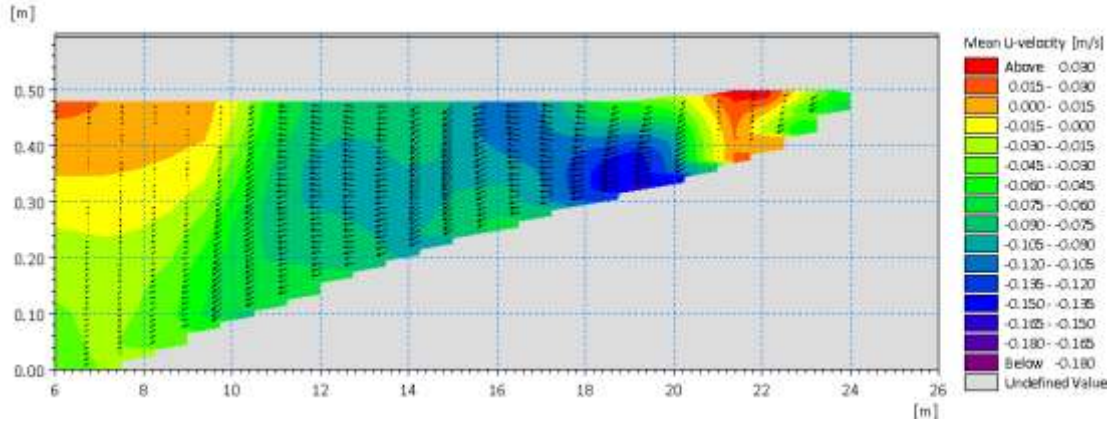

Figure 3.30 Mean u-velocity in the vertical plane along the centreline.

3.7 Porous Dam-break

3.7.1 Description

This test considers a dam-break through a porous structure. The model results are compared to the laboratory results given in Liu et al. (1999). The laboratory experiment was conducted in a wave tank that is 89.2cm long, 44cm wide and 58cm high. The porous structure is 29cm long, 44cm wide and 37cm high, and it is placed at x = 30.0-59.0cm, see Figure 3.31. A gate is placed 2cm to the left of the porous structure. On the left side of the gate the initial water depth, h, is about 25cm and on the right side of the gate it is 2.5cm. The porous structure consists of crushed rocks with an average diameter of 1.59cm, leading to a final porosity of 0.49. The experiment was started by removing the gate and hereby allowing the water to flow through the porous structure. The gate was removed manually within about 0.1s.

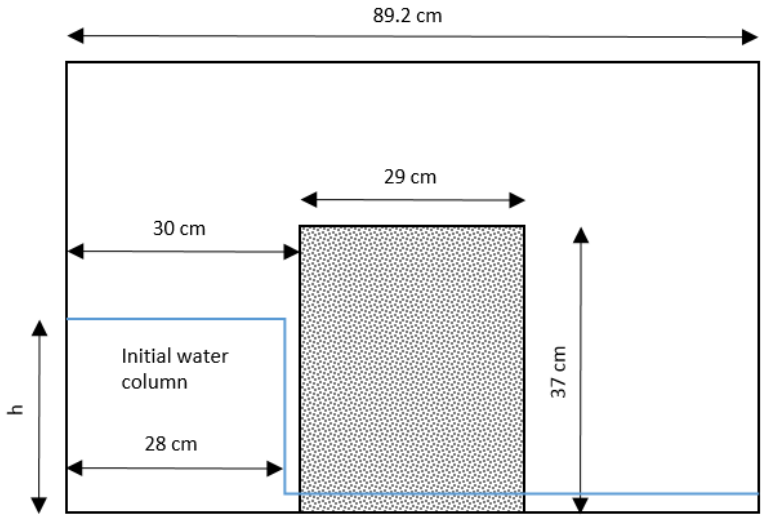

Figure 3.31 Initial porous Dam-Break setup.

3.7.2 Setup

For the numerical experiment, a structured mesh consisting of 223 quadrangular 2D elements is used. The grid spacing in the flow direction is $\Delta x = 0.4$m, whereas Δy is the full width of the tank. Vertically, the domain is discretized using 10 uniformly distributed layers in the sigma coordinate system, resulting in a total of 2230 elements being used in the simulation. The values of the linear and nonlinear friction parameters are set to $\alpha = 500$ and $\beta = 2$. And the oscillation period is set to 1s.

Simulations have been performed using the HLLC solver. Horizontal and vertical eddy are included using the k-epsilon formulation.

3.7.3 Results

The results of the numerical model are presented in Figure 3.32. For comparison, the laboratory results given in Liu et al. (1999) are plotted as red circles in the figure.

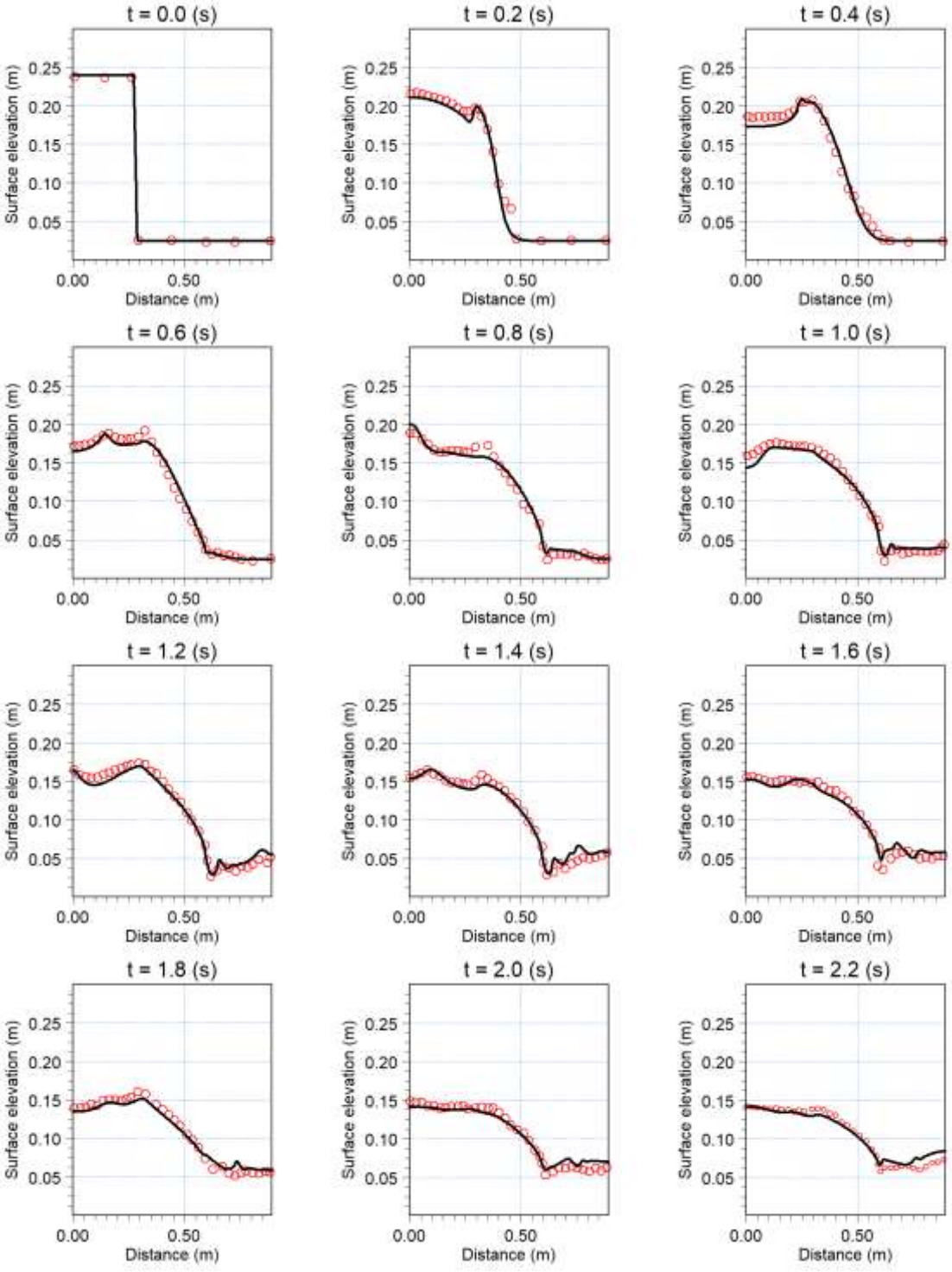

Figure 3.32 Comparison of the numerical computed surface elevation and the laboratory results given in Liu et al. (1999). Black line: Numerical results. Red circles: Laboratory results.

As illustrated in Figure 3.32 the numerical results agree very well with the measured lab results. The small deviations observed within the first second is probably due to the fact, that the gate is not instantaneously removed in the lab experiment, as it is the case in the numerical experiment.

3.8 Regular Waves Interacting with Vertical Porous Breakwater

3.8.1 Description

This test is validated against the experimental results presented in Lara et al. (2012). The test is conducted in a rectangular flume, which is 22m long, 0.585m wide and 0.78m high. A wave maker is positioned at the beginning of the flume, such that from the mean position of the wave maker to the end of the flume there is 20.595m. The wave maker has a stroke of ±0.45m. A porous structure being 0.24m long, 0.24m wide and 0.7m high is placed against the one side of the flume, such that the centre of the structure is located 11.519m from the mean position of the wave maker. Between the porous structure and the wall an impermeable block of plexiglass is placed. This block has a thickness of 0.06 m. See Figure 3.33 for an illustration of the experimental arrangement. The porous structure consists of crushed stones with a mean diameter of 0.0083m, leading to a final porosity of 0.48.

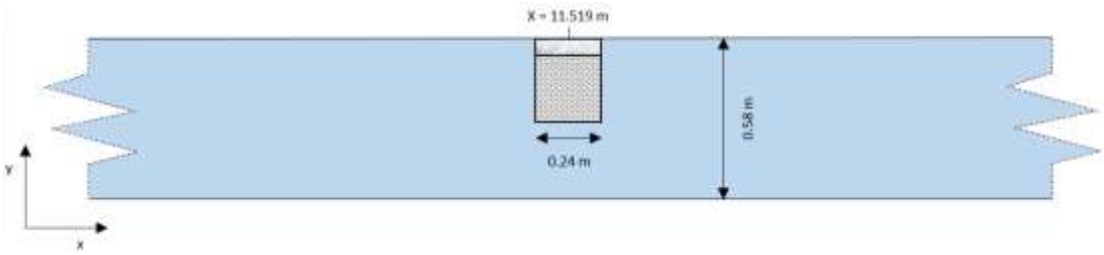

Figure 3.33 Subset of the experimental arrangement in the area around the porous structure.

The flume is equipped with a number of wave gauges, which are located as indicated in Table 3.2 and Figure 3.34.

Wave Gauge	x-coordinate (m)	y-coordinate (m)
W1	10.299	0.1
W2	10.299	0.485
W3	11.299	0.1
W4	11.299	0.385
W5	11.499	0.185
W6	11.739	0.1
W7	11.739	0.385
W8	12.039	0.1
W9	12.039	0.485
W10	12.439	0.285
W11	12.839	0.1
W12	12.839	0.485

Table 3.2 Wave gauge locations.

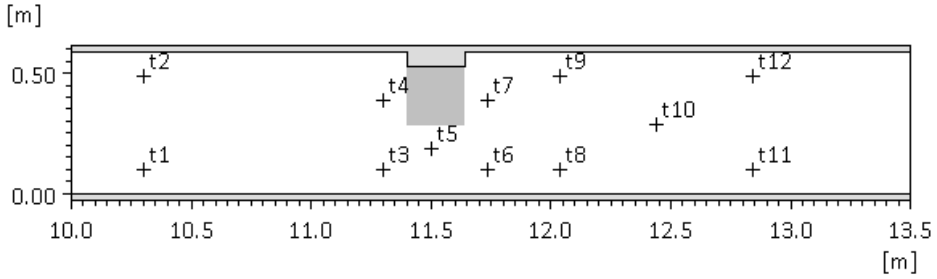

Figure 3.34 Wave gauge locations.

The experiment is run using regular waves with a period of 2s and a height of 0.06m. The mean water depth is 0.25m.

3.8.2 Setup

The numerical experiment uses quadrangular elements with a grid spacing in the range Δx = [0.02m, 0.04m] and Δy = 0.015m, resulting in a 2D mesh with 23460 elements. The grid is finest in the area around the porous structure, since this is the area of interest. A subset of the mesh is seen in Figure 3.35, which shows the mesh in the area around the structure. Vertically, 10 equidistant sigma layers are used, meaning that the total number of elements in the simulation is 234600.

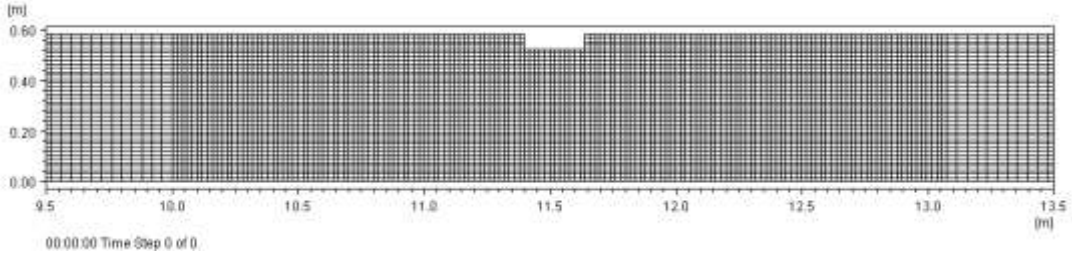

Figure 3.35 Subset of the computational mesh for the Vertical Porous Breakwater setup.

The waves are generated using a relaxation zone located at x = 1 m with a width of 0.8 m and using the stream function wave theory. The values of the linear and nonlinear friction parameters are set to α = 500 and β = 2.

Simulations have been performed using the HLLC solver. Horizontal and vertical eddy are included using the k-epsilon formulation.

3.8.3 Results

The numerical results for wave gauge 1-7 presented in Figure 3.36 are validated against the laboratory results given by Lara et al. (2012). The agreement is quite good both with respect to the phase and amplitude. Some discrepancies can be seen at the end of the time series, when the waves reflected from the end wall reach the area where the wave gauges are located.

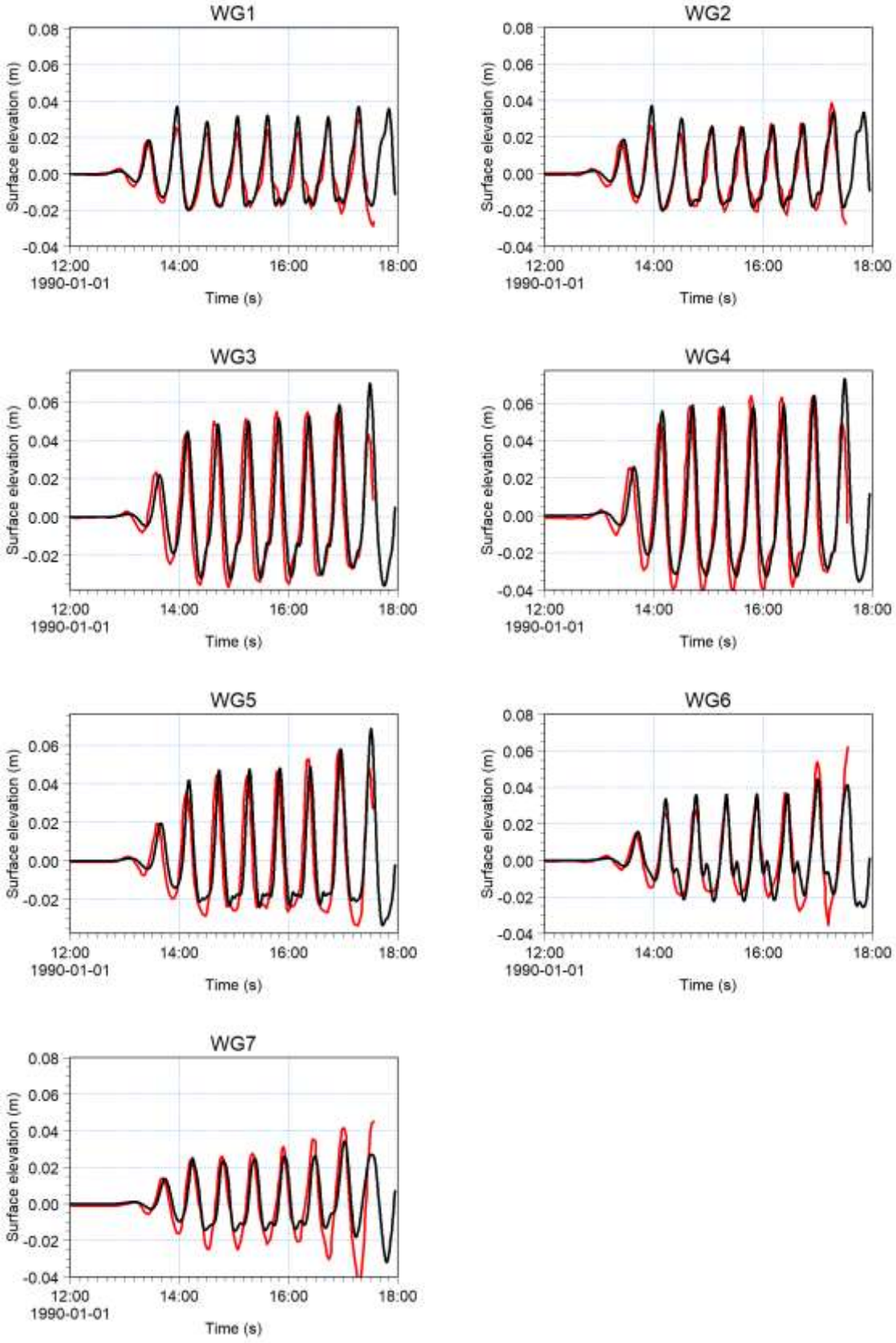

Figure 3.36 Computed and measured surface elevation at several locations. Black line: MIKE 3 Wave Model FM; Red line: Experimental data.

3.9 Wave Breaking over a Submerged Porous Breakwater

3.9.1 Description

The numerical results are compared to the experimental results presented in Hieu and Tanimoto (2006). The test is conducted in a rectangular flume, which is 18m long, 0.4m wide and 0.7m high. A submerged porous breakwater is placed in the flume. The breakwater is made of stones with a mean diameter of 0.025m, resulting in a final porosity of 0.45. The breakwater is 0.33m high and is 1.16 wide at the bottom and 0.3m wide at the top, see Figure 3.37. A wave maker is used to generate waves having a wave height and period of 0.092m and 1.6s, respectively. At the end of the flume a wave damper is placed to avoid wave reflection. The water depth is 0.376m. The origin of the (x,y,z)-coordinate system is placed at the breakwater.

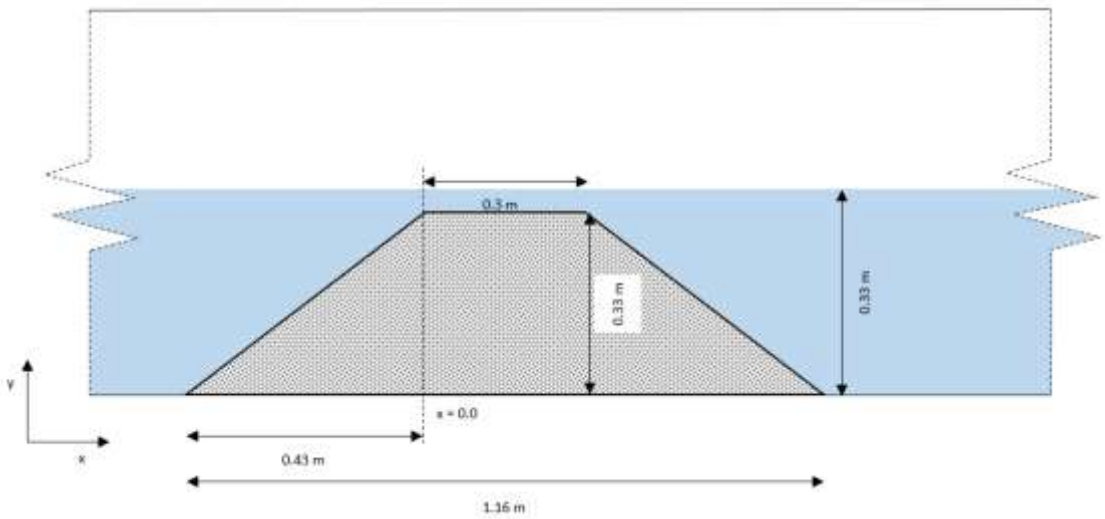

Figure 3.37 Subset of the area around the submerged and porous structure.

3.9.2 Setup

The numerical experiment considers a domain that is 20m long and 0.4m wide. The mesh consists of 1000 quadrangular elements with grid spacing $\Delta x = 0.02$m and $\Delta y = 0.4$m. Vertically, 40 equidistant sigma layers are used, meaning that the total number of elements in the simulation is 40000. The porous structure is placed at x = 0.0 and discretised as seen in Figure 3.38. The values of the linear and nonlinear friction parameters are set to $\alpha = 200$ and $\beta = 1.1$. The waves are generated using a relaxation zone, which is 2.0m wide and is placed at x = -7.63 and using stream function wave theory. A sponge layer is applied in the range x = [9.2m; 10.0m].

Simulations have been performed using the HLLC solver. Horizontal and vertical eddy are included using the k-epsilon formulation.

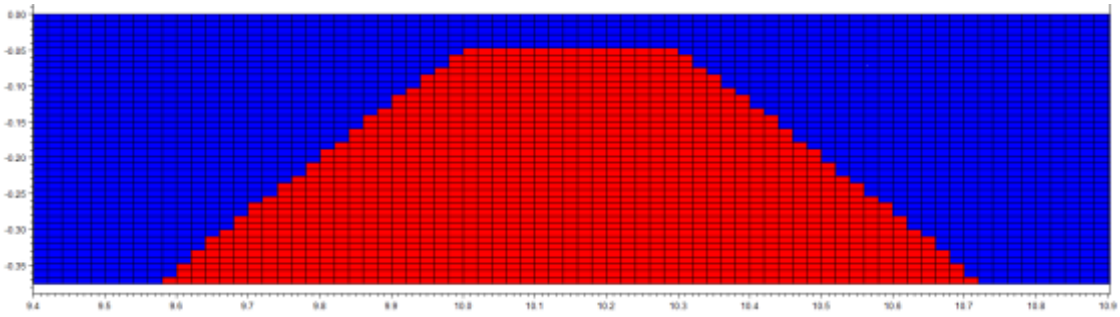

Figure 3.38 Discretised porous structure. Notice that the values on the x-axis are shifted by 10m on the figure compared to the numerical setup.

3.9.3 Results

The numerical results presented in Figure 3.39 are validated against the laboratory results given by Hieu and Tanimoto (2006). In general, the agreement is very good.

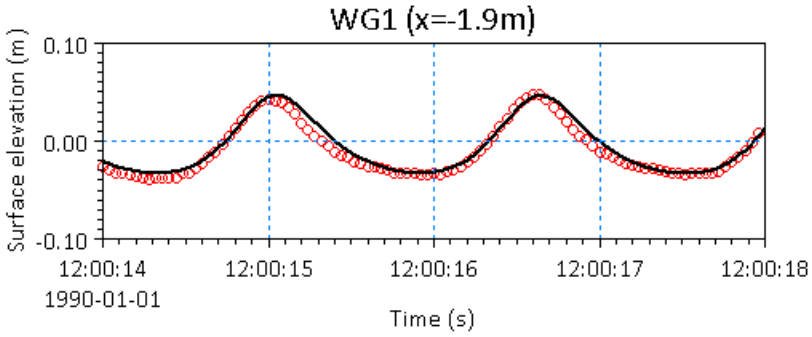

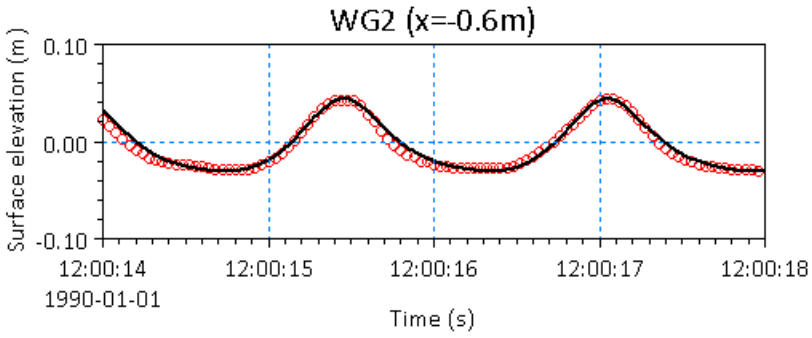

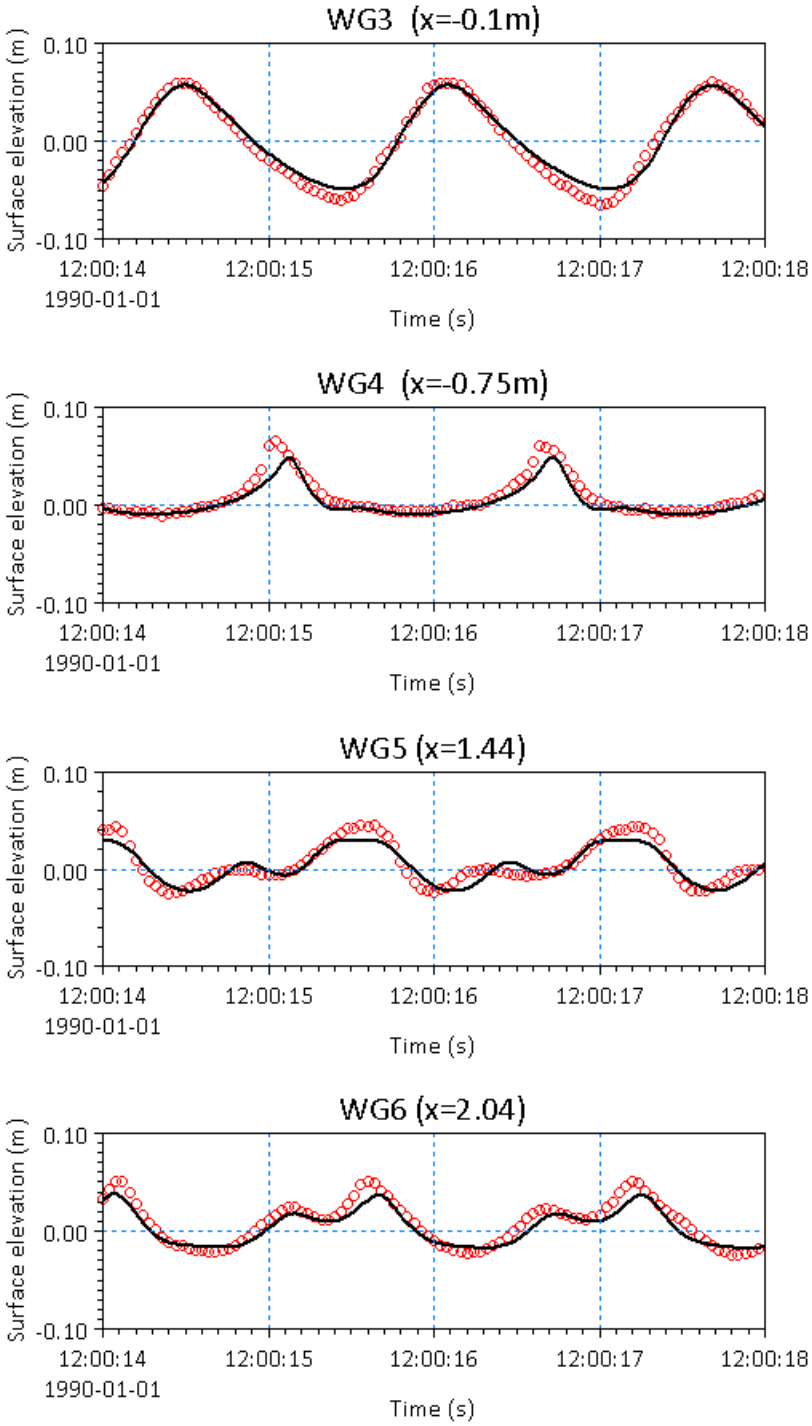

Figure 3.39 Computed and measured surface elevation at several locations. Blue line: MIKE 3 Wave Model FM; Red line: Experimental data.

3.10 Breakwater Overtopping

3.10.1 Description

Bruce et al. (2009) presented results from physical model tests of wave overtopping over breakwater structures. The main focus was on porous breakwaters with different types of armour layers. As a starting point a set of reference tests were made with an impermeable breakwater. This example shows how MIKE 3 Wave Model FM can be used to simulate wave overtopping over both an impermeable breakwater and porous breakwater based on these physical model tests. The example also shows the setup of a 3D porosity zone map and calculation of reflection coefficients from the porous breakwater.

3.10.2 Setup

The geometry of the model setup follows the flume experiments in Bruce et al. (2009). It consists of a flume with a length of 16m and a width of 1m. As the experiments can be considered to be two-dimensional the width of the flume is only resolved with one element. The length of the flume is resolved with elements having an edge length of 0.025m. The water depth is resolved with 10 non-equidistant sigma layers for the impermeable case and 30 non-equidistant sigma layers for the porous case.

For the impermeable breakwater case the toe of the impermeable breakwater is placed at a distance of 10m from the wave maker. The breakwater has a slope at 1:1.5 and the breakwater crest level is at 0.2812m (see Figure 3.40). For the porous breakwater case the water depth is constant in the whole domain, and the breakwater is modelled using a porosity map. In the experimental setup the breakwater was composed of three materials; core, filter layer and armour layer (see Figure 3.41). The thickness of the layers was related to the diameter of the applied armour units in the experiments. For the selected case with an armour layer composed of natural rocks, the stones had a diameter, d50 = 0.03m. The corresponding grain diameters for the filter and core material were 0.014m and 0.007m. The values of the linear and nonlinear friction parameters are set to $\alpha = 500$ and $\beta = 2$ and the porosity is set to 0.4 in all three zones. A close-up of the 3D porosity zone map is shown in Figure 3.42.

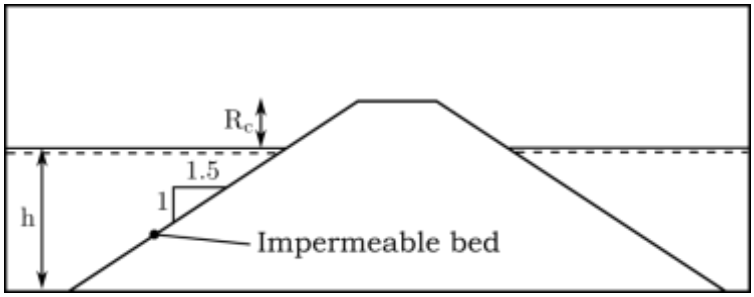

Figure 3.40 Sketch of the impermeable breakwater setup.

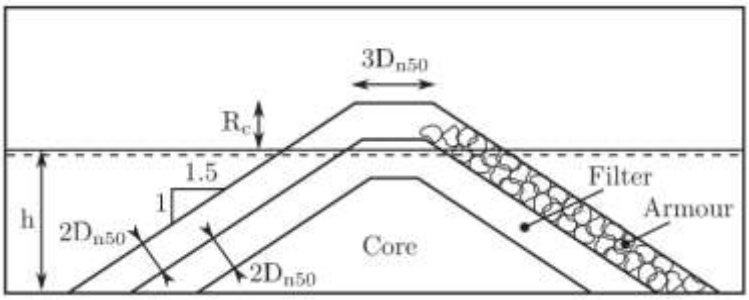

Figure 3.41 Sketch of the porous breakwater setup.

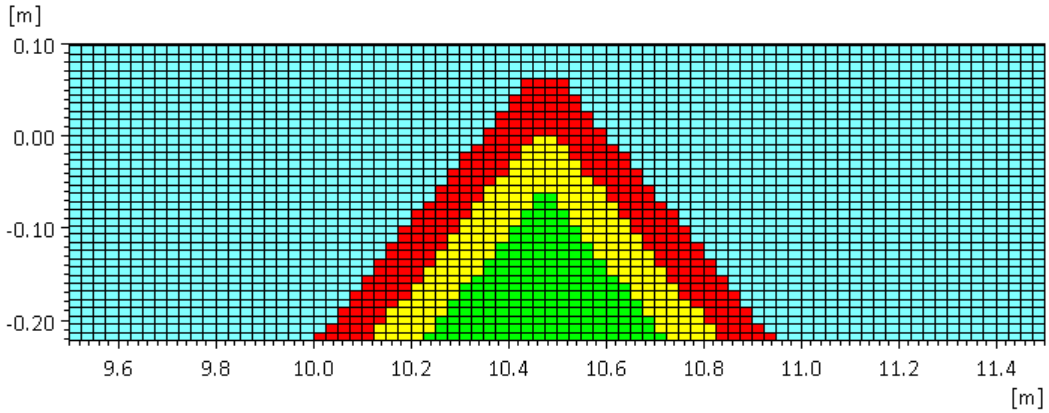

Figure 3.42 3D porosity map (dfsu-file) with three different porous zones.

Bruce et al. (2009) performed a number of experiments varying the water depth, and the wave conditions (wave height and wave period). In the present simulations for the impermeable breakwater case experiments, two different water depths are used: h=0.185m and h=0.222m. The breakwater crest level is at 0.2812m which gives a free board of R_c=0.0962m and R_c=0.0592m. Three different significant wave heights and peak periods are used: H_{m0}=[0.074m, 0.055m, 0.037m] and T_p=[1.56s, 1.16s, 0.97s]. This gives a total of 18 simulations. For the porous breakwater case, two different water depths are used: h=0.205m and h=0.237m which gives a free board of R_c=0.0762m and R_c=0.0442m. Three different significant wave heights and peak periods are used: H_{m0}=[0.111m, 0.074m, 0.055m] and T_p=[1.56s, 1.43s, 1.16s]. Again, this gives a total of 18 simulations. The incoming waves are specified using a relaxation zone: Line from (x,y)=(3.0m, 0.0m) to (x,y)=(3.0m, 1.0) and the width of the ramp-up zone is 3.0m. The simulation period was 1000s. Waves are generated as irregular waves based on the standard JONSWAP spectrum with a peak enhancement factor of γ = 3.3.

Horizontal and vertical eddy viscosity are applied using the k-ε formulation. The simulations are performed using the HLLC Riemann solver.

3.10.3 Results

The wave overtopping is measured by adding a discharge output line at the crest of the breakwater. This discharge line is setup to measure the flux and the accumulated discharge. The total accumulated discharge is converted to the overtopping rate by dividing by the length of the simulations, and made non-dimensional by the gravitational acceleration and significant wave height. The overtopping is presented as function of the non-dimensional free board. Figure 3.43 presents the overtopping rate for the impermeable breakwater compared to experimental data (Bruce et al. (2009)) and an empirical relation (see Bruce et al. (2009)). The model provides a good agreement between the simulated and experimental results. Figure 3.44 presents the overtopping rate for the porous breakwater compared to experimental data (Bruce et al. (2009)) and an empirical relation (see Bruce et al. (2009)). Here the overtopping is underestimated for small values of the peak period.

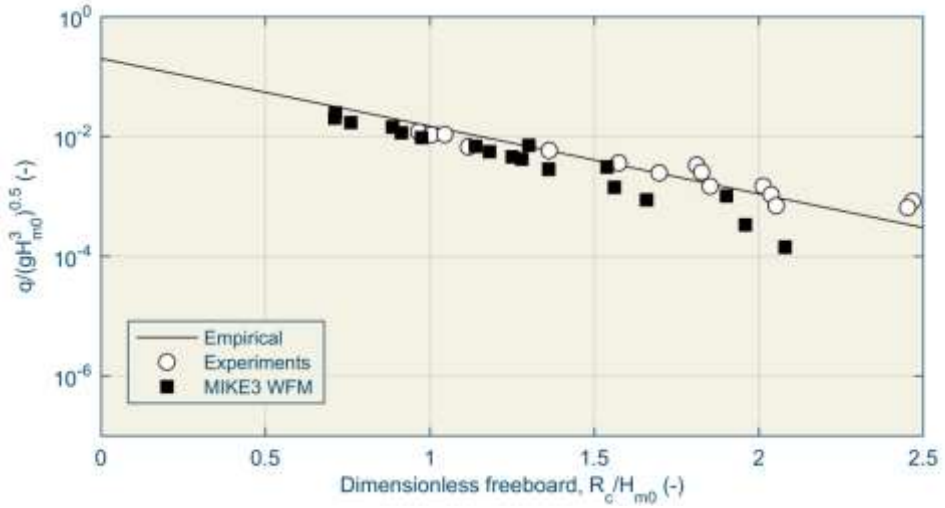

Figure 3.43 Comparisons between the numerical computed overtopping, experimental data by Bruce et al. (2009) and the empirical overtopping for the impermeable breakwater.

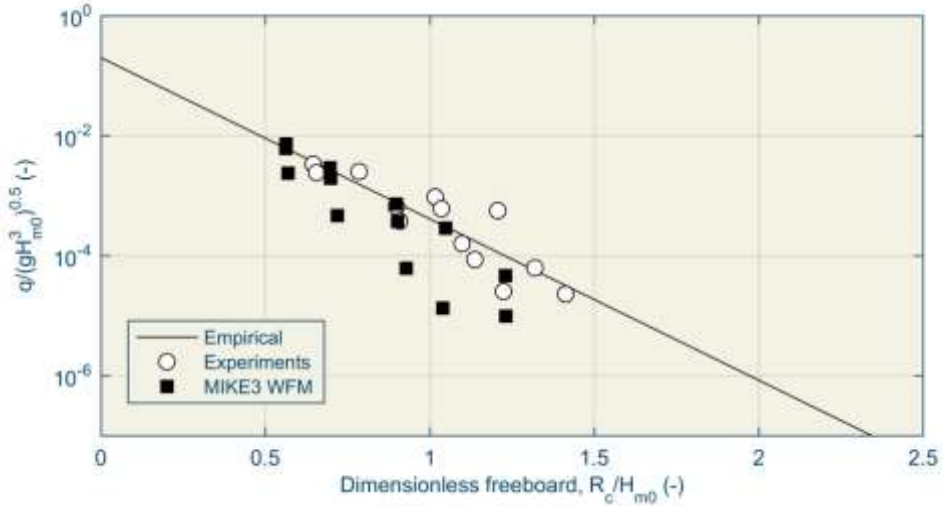

Figure 3.44 Comparisons between the numerical computed overtopping, experimental data by Bruce et al. (2009) and the empirical overtopping for the porous breakwater.

3.11 Submerged landslide

3.11.1 Description

This test considers a submerged landslide and the tsunami wave generated hereby. The simulated results are validated against the experimental results presented in Enet and Grilli (2007). The necessity for including the non-hydrostatic pressure when solving these kind of problems is made evident by a comparison between the simulated results from MIKE 3 Wave Model FM and MIKE 3 Flow Model FM, the latter having a hydrostatic pressure assumption.

The experimental setup in Enet and Grilli (2007) consists of a plane slope, 15m long and 3.7m wide, in an $\theta = 15° \pm 3'$ angle to the floor of the wave tank. The wave tank is 30m long, 3.7 m wide and 1.8m deep. The initial water depth is $h = 1.500 \pm 0.001m$
At time $t = 0.0$ a smooth, Gaussian-shaped, aluminum landslide geometry, placed on the plane slope, is quickly released and is sliding down the slope, thus creating a tsunami wave. A foam cushion at the bottom of the slope is used for stopping the landslide geometry. The landslide geometry is defined using truncated hyperbolic secant functions given in the two orthogonal directions, ξ and η

$$\zeta = \frac{T}{1-\varepsilon}(\mathrm{sech}(k_b\xi)\,\mathrm{sech}(k_w\eta) - \varepsilon)$$

with $k_b = 2C/b,\ \ k_w = 2C/w,\ \ C = \mathrm{acosh}\,(1/\varepsilon)$ where $\varepsilon =]0{,}1[$ is a truncation parameter. Here T, b and w is measured to $T = 0.082m,\ \ b = 0.395m$ and $w = 0.680m$. The value of ε is 0.717.

3.11.2 Setup

The numerical setup considers a domain that is 15m long and 3.7m wide. The mesh consists of 107987 triangular elements. Vertically, 5 non-equidistant sigma-layers are used, resulting in a total of 539935 elements in the simulation. The vertical distribution of the sigma-layers is done using the parameters $sigma_c = 0.1$, $theta = 2.0$ and $b = 0.0$. A sponge layer, 2.5m wide, is applied at the end of the domain. The initial water depth is set to $h = 1.5m$. The landslide itself is simulated using a time-varying bathymetry file, see Figure 3.45.

Simulations have been performed using the HLLC solver. Horizontal and vertical eddy are included using the k-epsilon formulation.

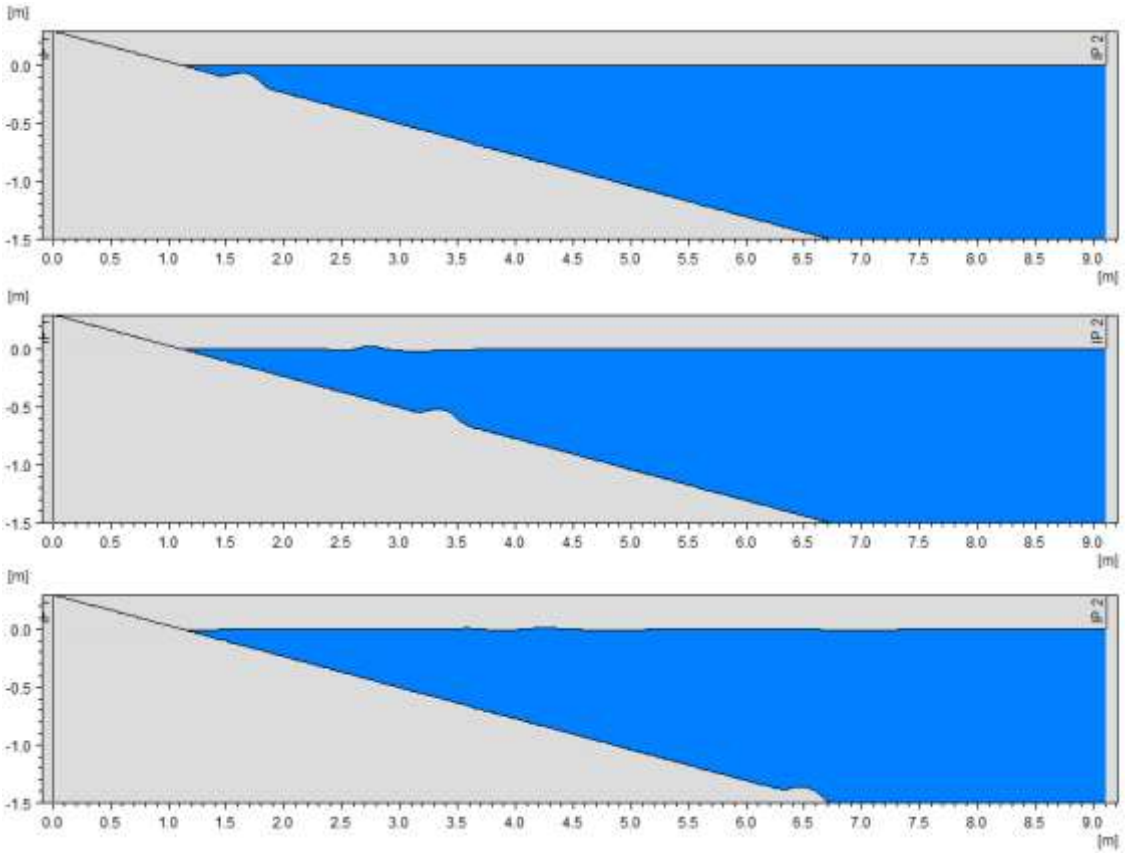

Figure 3.45 Bathymetry profile showing the landslide at time t = 0.0s, t = 2.0s and t = 4.0s.

3.11.3 Results

The numerical results presented in Figure 3.46 are validated against the experimental results given by Enet and Grilli (2007). The surface elevation is reported at four different (x, y) – positions in the domain using wave gauges: WG_1 = (0.56m, 0.0m), WG_2 = (1.469m, 0.35m), WG_3 = (1.929m, 0.0m) and WG_4 = (1.929m, 0.5m). In general, the agreement is very good. Furthermore, the comparison to MIKE 3 Flow Model FM shows that the non-hydrostatic pressure is essential for this type of simulation.

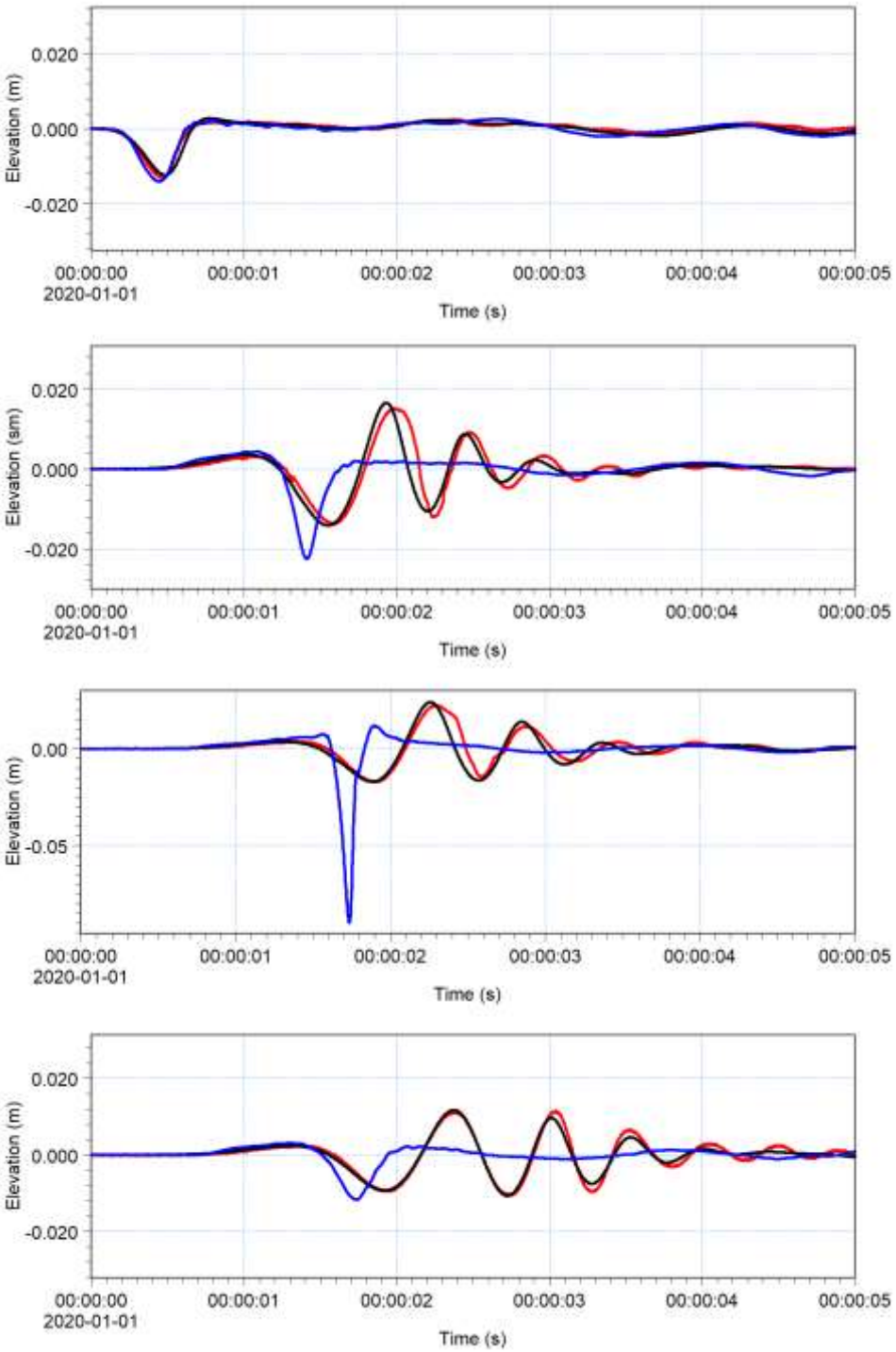

Figure 3.46 Surface elevation at the four wave gauges. From the top it is WG1, WG2, WG3 and WG4. Red line: measurements, Black line: MIKE 3 Wave Model FM (non-hydrostatic), Blue line: MIKE 3 Flow Model FM (hydrostatic).

4 References

/1/ Bruce, T., van der Meer, J. W., Franco, L., & Pearson, J. M. (2009). Overtopping performance of different armour units for rubble mound breakwaters. *Coastal Engineering*, *56*(2), 166–179.

/2/ Carrier, G. F and Greenspan, H. P. (1958): *Water Waves of Finite Amplitude on a Sloping Beach* Journal of Fluid Mechanics vol 4

/3/ Enet, F. and Grilli S., (2007), Experimental study of tsumami generation by three-dimensinal rigid underwater landslides, J. Waterway Port Coastal Ocean Eng. 133, 442-454.

/4/ Hamm, L., (1992a), Directional nearshore wave propagation over a rip channel: an experiment, *Pro. 23rd Int. Conf. Coastal Eng., Venice, Italy, 1992*, pp 226-239.

/5/ Hamm, L., (1992b), Random wave propagation in the nearshore zone: experiments in a directional wave basin, *Internal Report, MAST-G6M, SOGREAH*.

/6/ Hieu, P. D. and Tanimoto, K., (2006), Verification of a VOF-based two-phase flow model for wave breaking and wave-structure interactions, Ocean Eng., 33, 1565-1588.

/7/ Lara, J. L., del Jesus, M. and Losada, I. J., (2012), Three-dimensional interaction of waves and porous coastal structures. Part II: Experimental validation, *Coastal Eng.*, **64**, 26-46.

/8/ Liu, P.L.-F., Lin, P., Chang, K.-A. and Sakakiyama, T., (1999), Numerical modeling of wave interaction with porous structures, J. Waterw. Port Coast. Ocean Eng., 125, 322-330

/9/ Madsen, P. A., Murray, R. and Sørensen, O. R., (1991), A new form of the Boussinesq equations with improved linear dispersion characteristics. Part 1, *Coastal Eng.*, **15**, 371-388.

/10/ Madsen, P. A. and Sørensen, O. R., (1992), A new form of the Boussinesq equations with improved linear dispersion characteristic. Part II. A slowly-varying bathymetry, *Coastal Eng.*, **18**, 183-204.

/11/ Madsen, P. A., Schäffer, H. A. and Sørensen, O. R., (1997), Surf zone dynamics simulated by a Boussinesq type model. Part 1: Model description and cross-shore motion of regular waves, *Coastal Eng.*, **32**, 255-287.

/12/ Madsen, P. A., Sørensen, O. R. and Schäffer, H. A. (1997), Surf zone dynamics simulated by a Boussinesq type model. Part 2: Surf beat and swash oscillations for wave groups and irregular waves, *Coastal Eng*., 32 (4), 289-319.

/13/ Madsen, P. A. and Schäffer, H. A. (1999), A review of Boussinesq-type equations for surface gravity waves. In 'Advances in Coastal and Ocean Engineering', P.L.-F. Liu (ed.) 5, World Scientific Publ., pp 1-95.

/14/ Lai, Zhigang, C. Chen, G.W. Cowles and R.C. Beardsley (2010), A nonhydrostatic version of FVCOM: 1. Validation experiments, J. Geophys. Res., 115.

/15/ Luth, H.R., Klopman, G. and Kitau, N., (1994), “Project 13G: Kinematics of waves breaking partially on an offshore bar; LDV measurements for waves with and without a net onshore current”, Delft Hydraulics Report H1573, March 1994, 40pp.

/16/ Shi, F., Kirby, J. T., Ma, G., and Tehranirad, B. (2012). *Non-Hydrostatic Wave Model NHWAVE User’s Guide for Modeling Submarine Landslide Tsunami (Version 1.1)*. NHWAVE

/17/ Ting, F.C.K. and Kirby, J.T., (1994), Observation of undertow and turbulence in a laboratory surf zone, *Coastal Eng.*, **24**, 51-80.

/18/ Whalin, R. W., (1971), The limit of applicability of linear wave refraction theory in convergence zone, Res. Rep. H-71-3, U.S. Army Corps of Engineers, Waterways Expt. Station, Vicksburg, MS.